

Tangent Space Based Alternating Projections for Nonnegative Low Rank Matrix Approximation

Guangjing Song, Michael K. Ng, and Tai-Xiang Jiang,

Abstract—In this paper, we develop a new alternating projection method to compute nonnegative low rank matrix approximation for nonnegative matrices. In the nonnegative low rank matrix approximation method, the projection onto the manifold of fixed rank matrices can be expensive as the singular value decomposition is required. We propose to use the tangent space of the point in the manifold to approximate the projection onto the manifold in order to reduce the computational cost. We show that the sequence generated by the alternating projections onto the tangent spaces of the fixed rank matrices manifold and the nonnegative matrix manifold, converge linearly to a point in the intersection of the two manifolds where the convergent point is sufficiently close to optimal solutions. This convergence result based inexact projection onto the manifold is new and is not studied in the literature. Numerical examples in data clustering, pattern recognition and hyperspectral data analysis are given to demonstrate that the performance of the proposed method is better than that of nonnegative matrix factorization methods in terms of computational time and accuracy.

Index Terms—Alternating projection method, manifolds, tangent spaces, nonnegative matrices, low rank, nonnegativity.



1 INTRODUCTION

NONNEGATIVE data matrices appear in many data analysis applications. For instance, in image analysis, image pixel values are nonnegative and the associated nonnegative image data matrices can be formed for clustering and recognition [1], [2], [3], [4], [5], [6], [7], [8], [9], [10], [11], [12]. In text mining, the frequencies of terms in documents are nonnegative and the resulted nonnegative term-to-document data matrices can be constructed for clustering [13], [14], [15], [16]. In bioinformatics, nonnegative gene expression values are studied and nonnegative gene expression data matrices are generated for diseases and genes classification [17], [18], [19], [20], [21]. Low rank matrix approximation for nonnegative matrices plays a key role in all these applications. Its main purpose is to identify a latent feature space for objects representation. The classification, clustering or recognition analysis can be done by using these latent features.

Nonnegative Matrix Factorization (NMF) has emerged in 1994 by Paatero and Tapper [22] for performing environmental data analysis. The purpose of NMF is to decompose an input m -by- n nonnegative matrix $\mathbf{A} \in \mathbb{R}_+^{m \times n}$ into m -by- r nonnegative matrix $\mathbf{B} \in \mathbb{R}_+^{m \times r}$ and r -by- n nonnegative matrix $\mathbf{C} \in \mathbb{R}_+^{r \times n}$: $\mathbf{A} \approx \mathbf{BC}$, and more precisely

$$\min_{\mathbf{B}, \mathbf{C} \geq 0} \|\mathbf{A} - \mathbf{BC}\|_F^2, \quad (1)$$

where $\mathbf{B}, \mathbf{C} \geq 0$ means that each entry of \mathbf{B} and \mathbf{C} is nonnegative, $\|\cdot\|_F$ is the Frobenius norm of a matrix, and r (the low rank value) is smaller than m and n . Several researchers have proposed and developed algorithms for determining such nonnegative matrix factorization in the literature [4], [8], [23], [24], [25], [26], [27], [28], [29], [30], [31], [32]. Lee and Seung [8] proposed and developed NMF algorithms, and demonstrated that NMF has part-based representation which can be used for intuitive perception interpretation. For the development of NMF, we refer to the recently edited book [33].

In [34], Song and Ng proposed a new algorithm for computing Nonnegative Low Rank Matrix (NLRM) approximation for nonnegative matrices. The approach is completely different from NMF which has been studied for more than twenty five years. The new approach aims to find a nonnegative low rank matrix \mathbf{X} such that their difference is as small as possible. Mathematically, it can be formulated as the following optimization problem

$$\min_{\text{rank}(\mathbf{X})=r, \mathbf{X} \geq 0} \|\mathbf{A} - \mathbf{X}\|_F^2. \quad (2)$$

The convergence of the proposed algorithm is also proved and experimental results are shown that the minimized distance by the NLRM method can be smaller than that by the NMF method. Moreover, according to the ordering of singular values, the proposed method can identify important singular basis vectors, while this information may not be obtained in the classical NMF.

1.1 The Contribution

The algorithm proposed in [34] for computing the nonnegative low rank matrix approximation is based on using the alternating projections on the fixed-rank matrices manifold and the nonnegative matrices manifold. Note that the computational cost of the above alternating projection method is dominant by the calculation of the singular

- Guangjing Song is with School of Mathematics and Information Sciences, Weifang University, Weifang 261061, P.R. China. (email: sgjshu@163.com).
- M. K. Ng is with Department of Mathematics, The University of Hong Kong, Pokfulam, Hong Kong (e-mail: mng@maths.hku.hk). M. Ng's research supported in part by the HKRGC GRF 12306616, 12200317, 12300218, 12300519 and 17201020.
- T.-X. Jiang is with FinTech Innovation Center, School of Economic Information Engineering, Southwestern University of Finance and Economics, Chengdu, Sichuan, P.R.China (e-mail: taixiangjiang@gmail.com, jiangtx@swufe.edu.cn). T.-X. Jiang's research is supported in part by the Fundamental Research Funds for the Central Universities (JBK2001011, JBK2001035). The Corresponding Author.

value decomposition at each iteration. The computational workload of the singular value decomposition can be large especially when the size of the matrix is large. In this paper, we propose to use the tangent space of the point in the manifold to approximate the projection onto the manifold in order to reduce the computational cost. We show that the sequence generated by the alternating projections onto the tangent spaces of the fixed rank matrices manifold and the nonnegative matrix manifold, converge linearly to a point in the intersection of the two manifolds where the convergent point is sufficiently close to optimal solutions. Numerical examples will be presented to show that the computational time of the proposed tangent space based method is less than that of the original alternating projection method. Moreover, experimental results in data clustering, pattern recognition and hyperspectral data analysis, are given to demonstrate that the performance of the proposed method is better than that of other nonnegative matrix factorization methods in terms of computational time and accuracy.

The rest of this paper is organized as follows. In Section 2, we propose tangent space based alternating projection method. In Section 3, we show the convergence of the proposed method. In Section 4, numerical examples are given to show the advantages of the proposed method. Finally, some concluding remarks are given in Section 5.

2 NONNEGATIVE LOW RANK MATRIX APPROXIMATION

In this paper, we are interested in the $m \times n$ fixed-rank matrices manifold

$$\mathcal{M}_r := \{\mathbf{X} \in \mathbb{R}^{m \times n}, \text{rank}(\mathbf{X}) = r\}, \quad (3)$$

the $m \times n$ non-negativity matrices manifold

$$\mathcal{M}_n := \{\mathbf{X} \in \mathbb{R}^{m \times n}, \mathbf{X}_{ij} \geq 0, i = 1, \dots, m, j = 1, \dots, n\}, \quad (4)$$

and the $m \times n$ nonnegative fixed rank matrices manifold

$$\mathcal{M}_{rn} = \mathcal{M}_r \cap \mathcal{M}_n = \{\mathbf{X} \in \mathbb{R}^{m \times n}, \text{rank}(\mathbf{X}) = r, \mathbf{X}_{ij} \geq 0, i = 1, \dots, m, j = 1, \dots, n\}. \quad (5)$$

The proof of \mathcal{M}_{rn} is a manifold can be found in [34]. Let $\mathbf{X} \in \mathbb{R}^{m \times n}$ be an arbitrary matrix in the manifold \mathcal{M}_r . We set the singular value decomposition of \mathbf{X} as follows: $\mathbf{X} = \mathbf{U}\mathbf{\Sigma}\mathbf{V}^T$ where $\mathbf{U} \in \mathbb{R}^{m \times r}$, $\mathbf{\Sigma} \in \mathbb{R}^{r \times r}$, and $\mathbf{V} \in \mathbb{R}^{n \times r}$. It follows from Proposition 2.1 in [35] that the tangent space of \mathcal{M}_r at \mathbf{X} can be expressed as

$$T_{\mathcal{M}_r}(\mathbf{X}) = \{\mathbf{U}\mathbf{W}^T + \mathbf{Z}\mathbf{V}^T\}, \quad (6)$$

where $\mathbf{W} \in \mathbb{R}^{n \times r}$, $\mathbf{Z} \in \mathbb{R}^{m \times r}$ are arbitrary. Here \cdot^T denotes the transpose of a matrix. For a given m -by- n matrix \mathbf{Y} , the orthogonal projection of \mathbf{Y} onto the subspace $T_{\mathcal{M}_r}(\mathbf{X})$ can be written as

$$P_{T_{\mathcal{M}_r}(\mathbf{X})}(\mathbf{Y}) = \mathbf{U}\mathbf{U}^T\mathbf{Y} + \mathbf{Y}\mathbf{V}\mathbf{V}^T - \mathbf{U}\mathbf{U}^T\mathbf{Y}\mathbf{V}\mathbf{V}^T. \quad (7)$$

The alternating projection method studied in [34] is based on projecting the given nonnegative matrix onto the $m \times n$ fixed-rank matrices manifold \mathcal{M}_r and the non-negativity matrices manifold \mathcal{M}_n iteratively. The projection onto the

fixed rank matrix set \mathcal{M}_r is derived by the Eckart-Young-Mirsky theorem [36] which can be expressed as follows:

$$\pi_1(\mathbf{X}) = \sum_{i=1}^r \sigma_i(\mathbf{X})u_i(\mathbf{X})v_i^T(\mathbf{X}), \quad (8)$$

where $\sigma_i(\mathbf{X})$ are first r singular values of \mathbf{X} , and $u_i(\mathbf{X})$, $v_i(\mathbf{X})$ are their corresponding singular vectors. The projection onto the nonnegative matrix set \mathcal{M}_n is expressed as

$$\pi_2(\mathbf{X}) = \begin{cases} X_{ij}, & \text{if } X_{ij} \geq 0, \\ 0, & \text{if } X_{ij} < 0. \end{cases} \quad (9)$$

Moreover, \mathcal{M}_{rn} refers to the nonnegative fixed rank matrices manifold given as (5), and $\pi(\mathbf{X})$ refers to the closest matrix to the given nonnegative matrix \mathbf{X} , i.e.,

$$\pi(\mathbf{X}) = \underset{\mathbf{Y} \in \mathcal{M}_{rn}}{\text{argmax}} \|\mathbf{X} - \mathbf{Y}\|_F^2. \quad (10)$$

2.1 Projections Based on Tangent Spaces

Note that it can be expensive to project a matrix onto the fixed rank manifold by using the singular value decomposition. In this paper, we make use of tangent spaces and construct Tangent space based Alternating Projection (TAP) method to find nonnegative low rank matrix approximation such that the computational cost can be reduced compared with the original alternating projection method in [34]. In Figure 1 and Figure 2, we demonstrate the proposed TAP method. In the method, the given nonnegative matrix $\mathbf{X}_0 = \mathbf{A}$ was first projected onto the manifold \mathcal{M}_r to get a point \mathbf{X}_1 by π_1 , and then \mathbf{X}_2 is derived by projecting \mathbf{X}_1 onto the manifold \mathcal{M}_n by π_2 . The first two steps are same as the original alternating projection method [34]. According to the third step, the point \mathbf{X}_2 is first projected onto the tangent space at \mathbf{X}_1 of the manifold \mathcal{M}_r by the orthogonal projection $P_{T_{\mathcal{M}_r}(\mathbf{X}_1)}$, and then the derived point is projected from the tangent space to the manifold \mathcal{M}_r to get \mathbf{X}_3 . Thus the sequence can be derived as follows:

$$\begin{aligned} \mathbf{X}_0 &= \mathbf{A}, \mathbf{X}_1 = \pi_1(\mathbf{X}_0), \mathbf{X}_2 = \pi_2(\mathbf{X}_1), \\ \mathbf{X}_3 &= \pi_1(P_{T_{\mathcal{M}_r}(\mathbf{X}_1)}(\mathbf{X}_2)), \mathbf{X}_4 = \pi_2(\mathbf{X}_3), \dots, \\ \mathbf{X}_{2k+1} &= \pi_1(P_{T_{\mathcal{M}_r}(\mathbf{X}_{2k-1})}(\mathbf{X}_{2k})), \mathbf{X}_{2k+2} = \pi_2(\mathbf{X}_{2k+1}), \dots \end{aligned}$$

where $P_{T_{\mathcal{M}_r}(\mathbf{X}_{2k-1})}(\mathbf{X}_{2k})$ denotes the orthogonal projections of \mathbf{X}_{2k} onto the tangent space of \mathcal{M}_r at \mathbf{X}_{2k-1} . The algorithm is summarized in Algorithm 1.

Algorithm 1 Tangent spaces based Alternating Projection (TAP) Method

Input: Given a nonnegative matrix $\mathbf{A} \in \mathbb{R}^{m \times n}$ this algorithm computes nearest rank- r nonnegative matrix.

- 1: Initialize $\mathbf{X}_0 = \mathbf{A}$;
- 2: $\mathbf{X}_1 = \pi_1(\mathbf{X}_0)$ and $\mathbf{Y}_1 = \pi_2(\mathbf{X}_1)$
- 3: for $k=1,2,\dots$,
- 4: $\mathbf{X}_{k+1} = \pi_1(P_{T_{\mathcal{M}_r}(\mathbf{X}_k)}(\mathbf{Y}_k))$;
- 5: $\mathbf{Y}_{k+1} = \pi_2(\mathbf{X}_{k+1})$;
- 6: **end**

Output: \mathbf{X}_k when the stopping criterion is satisfied.

Let us analyze the computational cost of TAP method in each iteration. Let $\mathbf{X}_k = \mathbf{U}_k\mathbf{\Sigma}_k\mathbf{V}_k^T$ be the skinny SVD

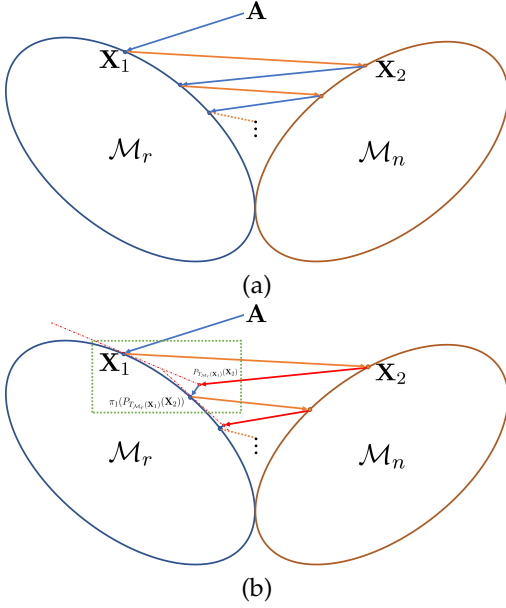


Fig. 1. The comparison between (a) the original alternating projection method and (b) the proposed TAP method.

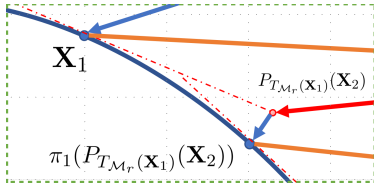


Fig. 2. The zoomed region in Figure 1(b).

decomposition of \mathbf{X}_k . By (6), the tangent space of \mathcal{M}_r at \mathbf{X}_k can be expressed as

$$T_{\mathcal{M}_r}(\mathbf{X}_k) = \{\mathbf{U}_k \mathbf{W}^T + \mathbf{Z} \mathbf{V}_k^T\},$$

where $\mathbf{W} \in \mathbb{R}^{n \times r}$, $\mathbf{Z} \in \mathbb{R}^{m \times r}$ are arbitrary. According to (10), the orthogonal projection of \mathbf{Y}_k onto the subspace $T_{\mathcal{M}_r}(\mathbf{X}_k)$ can be written as follows:

$$P_{T_{\mathcal{M}_r}(\mathbf{X}_k)}(\mathbf{Y}_k) = \mathbf{U}_k \mathbf{U}_k^T \mathbf{Y}_k + \mathbf{Y}_k \mathbf{V}_k \mathbf{V}_k^T - \mathbf{U}_k \mathbf{U}_k^T \mathbf{Y}_k \mathbf{V}_k \mathbf{V}_k^T.$$

Now it is required to compute the SVD of the projected matrix $P_{T_{\mathcal{M}_r}(\mathbf{X}_k)}(\mathbf{Y}_k)$ with smaller size. Suppose that the QR decompositions of $(\mathbf{I} - \mathbf{U}_k \mathbf{U}_k^T) \mathbf{Y}_k \mathbf{V}_k$ and $(\mathbf{I} - \mathbf{V}_k \mathbf{V}_k^T) \mathbf{Y}_k \mathbf{U}_k$ are given as follows:

$$(\mathbf{I} - \mathbf{U}_k \mathbf{U}_k^T) \mathbf{Y}_k \mathbf{V}_k = \mathbf{Q}_k \mathbf{R}_k$$

and

$$(\mathbf{I} - \mathbf{V}_k \mathbf{V}_k^T) \mathbf{Y}_k^T \mathbf{U}_k = \hat{\mathbf{Q}}_k \hat{\mathbf{R}}_k,$$

respectively. Recall that $\mathbf{U}_k^T \mathbf{Q}_k = \mathbf{V}_k^T \hat{\mathbf{Q}}_k = \mathbf{0}$ and then by a

direct computation, we have

$$\begin{aligned} & P_{T_{\mathcal{M}_r}(\mathbf{X}_k)}(\mathbf{Y}_k) \\ &= \mathbf{U}_k \mathbf{U}_k^T \mathbf{Y}_k (\mathbf{I} - \mathbf{V}_k \mathbf{V}_k^T) + (\mathbf{I} - \mathbf{U}_k \mathbf{U}_k^T) \mathbf{Y}_k \mathbf{V}_k \mathbf{V}_k^T \\ &\quad + \mathbf{U}_k \mathbf{U}_k^T \mathbf{Y}_k \mathbf{V}_k \mathbf{V}_k^T \\ &= \mathbf{U}_k \hat{\mathbf{R}}_k^T \hat{\mathbf{Q}}_k^T + \mathbf{Q}_k \mathbf{R}_k \mathbf{V}_k^T + \mathbf{U}_k \mathbf{U}_k^T \mathbf{Y}_k \mathbf{V}_k \mathbf{V}_k^T \\ &= (\mathbf{U}_k \quad \mathbf{Q}_k) \begin{pmatrix} \mathbf{U}_k^T \mathbf{Y}_k \mathbf{V}_k & \hat{\mathbf{R}}_k^T \\ \mathbf{R}_k & \mathbf{0} \end{pmatrix} \begin{pmatrix} \mathbf{V}_k^T \\ \hat{\mathbf{Q}}_k^T \end{pmatrix} \\ &:= (\mathbf{U}_k \quad \mathbf{Q}_k) \mathbf{M}_k \begin{pmatrix} \mathbf{V}_k^T \\ \hat{\mathbf{Q}}_k^T \end{pmatrix}. \end{aligned}$$

Let $\mathbf{M}_k = \Psi_k \Gamma_k \Phi_k^T$ be the SVD of \mathbf{M}_k which can be computed using $O(r^3)$ flops since \mathbf{M}_k is a $2r \times 2r$ matrix. Note that $(\mathbf{U}_k, \mathbf{Q}_k)$ and $(\mathbf{V}_k, \hat{\mathbf{Q}}_k)$ are orthogonal, then the SVD of $P_{T_{\mathcal{M}_r}(\mathbf{X}_k)}(\mathbf{Y}_k) = \Omega_k \Theta_k \Upsilon_k^T$ can be computed by

$$\Omega_k = (\mathbf{U}_k, \mathbf{Q}_k) \Psi_k, \Theta_k = \Gamma_k \text{ and } \Upsilon_k = (\mathbf{V}_k, \hat{\mathbf{Q}}_k) \Phi_k.$$

It follows that the overall computational cost of $\pi_1(P_{T_{\mathcal{M}_r}(\mathbf{X}_k)}(\mathbf{Y}_k))$ can be expressed as two matrix-matrix multiplications. In addition, the calculation procedure involves the QR decomposition of two matrices of sizes $m \times r$ and $n \times r$ matrices, and the SVD of a matrix of size $2r \times 2r$. The total cost per iteration is $4mnr + O(r^2m + r^2n + r^3)$. In contrast, the computation of the best rank- r approximation of a non-structured $m \times n$ matrix costs $O(mnr) + mn$ flops where the constant in front of mnr can be very large. In practice, the cost per iteration of the proposed TAP method is less than that of original alternating projection method. In Section 4, numerical examples will be given to demonstrate the total computational time of the proposed TAP method is less than that of the original alternating projection method.

3 THE CONVERGENCE ANALYSIS

In this section, we study the convergence of the proposed TAP method in Algorithm 1. We note that the convergence result of the original alternating projection method has been established in [37]. The key concept is the angle of a point in the intersection of two manifolds. In our setting, the angle $\alpha(\mathbf{B})$ of $\mathbf{B} \in \mathcal{M}_{r,n}$ where

$$\alpha(\mathbf{B}) = \cos^{-1}(\sigma(\mathbf{B})) \quad (11)$$

and

$$\sigma(\mathbf{B}) = \lim_{\xi \rightarrow 0} \sup_{\mathbf{B}_1 \in F_1^\xi(\mathbf{B}), \mathbf{B}_2 \in F_2^\xi(\mathbf{B})} \left\{ \frac{\langle \mathbf{B}_1 - \mathbf{B}, \mathbf{B}_2 - \mathbf{B} \rangle}{\|\mathbf{B}_1 - \mathbf{B}\|_F \|\mathbf{B}_2 - \mathbf{B}\|_F} \right\},$$

with

$$F_1^\xi(\mathbf{B}) = \{\mathbf{B}_1 \mid \mathbf{B}_1 \in \mathcal{M}_r \setminus \mathbf{B}, \|\mathbf{B}_1 - \mathbf{B}\|_F \leq \xi, \mathbf{B}_1 - \mathbf{B} \perp T_{\mathcal{M}_r \cap \mathcal{M}_n}(\mathbf{B})\},$$

$$F_2^\xi(\mathbf{B}) = \{\mathbf{B}_2 \mid \mathbf{B}_2 \in \mathcal{M}_n \setminus \mathbf{B}, \|\mathbf{B}_2 - \mathbf{B}\|_F \leq \xi, \mathbf{B}_2 - \mathbf{B} \perp T_{\mathcal{M}_r \cap \mathcal{M}_n}(\mathbf{B})\},$$

and $T_{\mathcal{M}_r \cap \mathcal{M}_n}(\mathbf{B})$ is the tangent space of $\mathcal{M}_r \cap \mathcal{M}_n$ at point \mathbf{B} . The angle is calculated based on the two points belonging \mathcal{M}_r and \mathcal{M}_n respectively. A point \mathbf{B} in $\mathcal{M}_{r,n}$ is nontangential if $\alpha(\mathbf{B})$ has a positive angle, i.e., $0 \leq \sigma(\mathbf{B}) < 1$.

In the following, we list the main convergence results of Algorithm 1 that has been studied in the literature.

Theorem 3.1. *Let \mathcal{M}_r , \mathcal{M}_n and \mathcal{M}_{rn} be given as (3), (4) and (5), the projections onto \mathcal{M}_r and \mathcal{M}_n be given as (8)-(9), respectively. Suppose that $\mathbf{P} \in \mathcal{M}_{rn}$ is a non-tangential intersection point, then for any given $\epsilon > 0$ and $1 > c > \sigma(\mathbf{P})$, there exist an $\xi > 0$ such that for any $\mathbf{A} \in \text{Ball}(\mathbf{P}, \xi)$ (the ball neighborhood of \mathbf{P} with radius ξ contains the given nonnegative matrix \mathbf{A}), the sequence \mathbf{X}_k generated by Algorithm 1 converges to a point $\mathbf{X}_\infty \in \mathcal{M}_{rn}$, and satisfy*

- (1) $\|\mathbf{X}_\infty - \pi(\mathbf{A})\|_F \leq \epsilon \|\mathbf{A} - \pi(\mathbf{A})\|_F$,
- (2) $\|\mathbf{X}_\infty - \mathbf{X}_k\|_F \leq \text{const} \cdot c^k \|\mathbf{A} - \pi(\mathbf{A})\|_F$,

where $\pi(\mathbf{A})$ is defined in (10).

Here we first present and establish some preliminary results and then give the proof of Theorem 3.1. These results are used to estimate the approximation when tangent spaces are used in the projections.

Lemma 3.2 (Proposition 4.3 and Theorem 4.1 in [37]). *Let $\mathbf{P} \in \mathcal{M}_r$ be given and π_1, π be defined as (8) and (10). For each $0 < \epsilon < \frac{3}{5}$, there exist an $s(\epsilon) > 0$ and an $\varepsilon(\epsilon) > 0$, such that for any given $\mathbf{Z} \in \text{Ball}(\mathbf{P}, s(\epsilon))$,*

$$\|\pi_1(\mathbf{Z}) - P_{T_{\mathcal{M}_r}(\pi(\mathbf{Z}))}(\mathbf{Z})\|_F < 4\sqrt{\epsilon} \|\mathbf{Z} - \pi(\mathbf{Z})\|_F, \quad (12)$$

and

$$\|\pi(\pi_1(\mathbf{Z})) - \pi(\mathbf{Z})\|_F < \varepsilon(\epsilon) \|\mathbf{Z} - \pi(\mathbf{Z})\|_F. \quad (13)$$

Lemma 3.3 (Proposition 2.4 in [37]). *Let $\mathbf{P} \in \mathcal{M}_r$ be given. For each $\epsilon > 0$, there exists $s > 0$ such that for all $\mathbf{C} \in \text{Ball}(\mathbf{P}, s) \cap \mathcal{M}_r$, we have:*

- (i) $\min_{\mathbf{D}' \in T_{\mathcal{M}_r}(\mathbf{C})} \|\mathbf{D} - \mathbf{D}'\|_F \leq \epsilon \|\mathbf{D} - \mathbf{C}\|_F, \forall \mathbf{D} \in \text{Ball}(\mathbf{P}, s) \cap \mathcal{M}_r$.
- (ii) $\|\mathbf{D} - \pi_1(\mathbf{D})\|_F \leq \epsilon \|\mathbf{D} - \mathbf{C}\|_F, \forall \mathbf{D} \in \text{Ball}(\mathbf{P}, s) \cap T_{\mathcal{M}_r}(\mathbf{C})$.

Next we can estimate the distance with respect to the other point in \mathcal{M}_r instead of using $\pi(\mathbf{Z})$. The following results which are proved in Appendix A.1 are needed.

Lemma 3.4. *Let $\mathbf{P} \in \mathcal{M}_r$ be given, $P_{T_{\mathcal{M}_r}}$ and π_1 be given as (7) and (8). For each $0 < \epsilon < \frac{3}{5}$, there exist an $s(\epsilon) > 0$ and a point $\mathbf{Q} \in \text{Ball}(\mathbf{P}, s(\epsilon)) \cap \mathcal{M}_r$ such that for any given $\mathbf{Z} \in \text{Ball}(\mathbf{P}, s(\epsilon))$, we have*

$$\|\pi_1(\mathbf{Z}) - P_{T_{\mathcal{M}_r}(\mathbf{Q})}(\mathbf{Z})\|_F < 4\sqrt{\epsilon} \|\mathbf{Z} - \mathbf{Q}\|_F. \quad (14)$$

Lemma 3.5 (Theorem 4.5 in [37]). *Suppose \mathbf{P} is a nontangential point with $\sigma(\mathbf{P}) < c$. Then there exists an $s > 0$ such that for all $\mathbf{Z} \in \mathcal{M}_n \cap \text{Ball}(\mathbf{P}, s)$, we have*

$$\|\pi_1(\mathbf{Z}) - \pi(\mathbf{Z})\|_F < c \|\mathbf{Z} - \pi(\mathbf{Z})\|_F. \quad (15)$$

Next we would like to estimate the distance between $\pi(\pi_1(P_{T_{\mathcal{M}_r}(\mathbf{Q})}(\mathbf{Z})))$ and $\pi(\mathbf{Z})$ where they are on the manifold \mathcal{M}_{rn} .

Lemma 3.6. *Let $\mathbf{P} \in \mathcal{M}_{rn}$ be given. For each $0 < \epsilon < \frac{3}{5}$, there exist $\varepsilon_1(\epsilon) > 0$, $\varepsilon_2(\epsilon) > 0$ and $s_1(\epsilon) > 0$ such that for all $\mathbf{Z} \in \text{Ball}(\mathbf{P}, s_1(\epsilon))$,*

$$\begin{aligned} \|\pi(\pi_1(P_{T_{\mathcal{M}_r}(\mathbf{Q})}(\mathbf{Z}))) - \pi(\mathbf{Z})\|_F &\leq \varepsilon_1(\epsilon) \|\mathbf{Z} - \pi(\mathbf{Z})\|_F \\ &+ \varepsilon_2(\epsilon) \|\mathbf{Q} - \pi(\mathbf{Z})\|_F, \end{aligned}$$

where $\mathbf{Q} \in \mathcal{M}_r \cap \text{Ball}(\mathbf{P}, s_1(\epsilon))$.

The proof of Lemma 3.6 can be found in Appendix A.2. According to Lemma 3.6, if $\mathbf{Z} = \pi_2(\mathbf{Q})$, then

$$\|\mathbf{Z} - \mathbf{Q}\|_F = \|\mathbf{Q} - \pi_2(\mathbf{Q})\|_F \leq \|\mathbf{Q} - \pi(\mathbf{Z})\|_F$$

by noting that $\pi(\mathbf{Z}) \in \mathcal{M}_n$, and

$$\begin{aligned} &\|\pi(\pi_1(P_{T_{\mathcal{M}_r}(\mathbf{Q})}(\mathbf{Z}))) - \pi(\mathbf{Z})\|_F \\ &\leq 8\alpha\sqrt{\epsilon} \|\mathbf{Z} - \mathbf{Q}\|_F + \varepsilon(\epsilon) \|\mathbf{Z} - \pi(\mathbf{Z})\|_F \\ &\leq \varepsilon_1(\epsilon) \|\mathbf{Z} - \pi(\mathbf{Z})\|_F + \varepsilon_2(\epsilon) \|\mathbf{Q} - \pi(\mathbf{Z})\|_F, \end{aligned}$$

where $\varepsilon_1(\epsilon) = \varepsilon(\epsilon)$ and $\varepsilon_2(\epsilon) = 8\alpha\sqrt{\epsilon}$.

In order to prove the convergence of Algorithm 1, we need to estimate the distance between $\pi_1(P_{T_{\mathcal{M}_r}(\mathbf{Q})}(\mathbf{Z}))$ and $\pi(\mathbf{Z})$. The proof can be found in Appendix A.3.

Lemma 3.7. *Suppose \mathbf{P} is a nontangential point in \mathcal{M}_{rn} with $\sigma(\mathbf{P}) < c$, and $\mathbf{Q} \in \mathcal{M}_r$. Then there exists an $s > 0$ such that when $\mathbf{Z} = \pi_2(\mathbf{Q}) \in \mathcal{M}_n \cap \text{Ball}(\mathbf{P}, s)$ and $P_{T_{\mathcal{M}_r}(\mathbf{Q})}(\mathbf{Z}) \in T_{\mathcal{M}_r}(\mathbf{Q}) \cap \text{Ball}(\mathbf{P}, s)$, we have*

$$\|\pi_1(P_{T_{\mathcal{M}_r}(\mathbf{Q})}(\mathbf{Z})) - \pi(\mathbf{Z})\|_F < c \|\mathbf{Z} - \pi(\mathbf{Z})\|_F. \quad (16)$$

With the above preliminaries, we give the proof of Theorem 3.1.

Proof of Theorem 3.1 Suppose that $\epsilon < 1$, and set $\sigma(\mathbf{P}) < c < 1$ and

$$\varepsilon = \frac{1-c}{2(3-c)}\epsilon, \quad \varepsilon_2(\epsilon) = \frac{1-c}{2+2\alpha}\epsilon,$$

where α is a constant given as in (30). It follows Lemma 3.5-3.7 that there exist some possibly distinct radii that guarantee (15)-(16) are satisfied. Let s denote the minimum of these possibly radii and pick $r < \frac{s(1-\epsilon)}{4(2+\epsilon)}$, so that $\pi(\text{Ball}(\mathbf{P}, r)) \subseteq \text{Ball}(\mathbf{P}, \frac{s}{4})$. Then $\|\pi(\mathbf{A}) - \mathbf{P}\|_F < \frac{s}{4}$ follows from the latter condition. Denote $l = \|\mathbf{A} - \pi(\mathbf{A})\|_F$ and note that

$$l = \|\mathbf{A} - \mathbf{P} + \mathbf{P} - \pi(\mathbf{A})\|_F \leq \|\mathbf{A} - \mathbf{P}\|_F + \|\mathbf{P} - \pi(\mathbf{A})\|_F \leq r + \frac{s}{4}.$$

As $\pi(\mathbf{A}) \in \mathcal{M}_{rn}$ and note that $\mathbf{X}_1 = \pi_1(\mathbf{A})$, we have

$$\|\mathbf{X}_1 - \mathbf{A}\|_F = \|\pi_1(\mathbf{A}) - \mathbf{A}\|_F \leq \|\pi(\mathbf{A}) - \mathbf{A}\|_F = l$$

and

$$\begin{aligned} \|\mathbf{X}_1 - \pi(\mathbf{X}_1)\|_F &\leq \|\mathbf{X}_1 - \pi(\mathbf{A})\|_F \\ &\leq \|\mathbf{X}_1 - \mathbf{A}\|_F + \|\mathbf{A} - \pi(\mathbf{A})\|_F \leq 2l. \end{aligned}$$

In order to prove $\{\mathbf{X}_k\}$ derived by Algorithm 1 is convergent, we need to prove $\{\mathbf{X}_k\}$ is a Cauchy sequence. By Lemma 3.7, there exist an c_1 such that

$$\begin{aligned} \|\mathbf{X}_{2k+1} - \pi(\mathbf{X}_{2k+1})\|_F &\leq \|\mathbf{X}_{2k+1} - \pi(\mathbf{X}_{2k})\|_F \\ &\leq c_1 \|\mathbf{X}_{2k} - \pi(\mathbf{X}_{2k})\|_F. \end{aligned} \quad (17)$$

In addition, by Lemma 3.5, there exist an c_2 such that

$$\begin{aligned} \|\mathbf{X}_{2k} - \pi(\mathbf{X}_{2k})\|_F &\leq \|\mathbf{X}_{2k} - \pi(\mathbf{X}_{2k-1})\|_F \\ &\leq c_2 \|\mathbf{X}_{2k-1} - \pi(\mathbf{X}_{2k-1})\|_F. \end{aligned} \quad (18)$$

Set $c = \max\{c_1, c_2\}$, combine (17) and (18) together gives

$$\|\mathbf{X}_k - \pi(\mathbf{X}_k)\|_F \leq c \|\mathbf{X}_{k-1} - \pi(\mathbf{X}_{k-1})\|_F. \quad (19)$$

Then $\{\mathbf{X}_k\}$ is a Cauchy sequence if and only if

$$\{\mathbf{X}_k\}_{k=1}^\infty \subseteq \text{Ball}(\mathbf{P}, s) \quad (20)$$

is satisfied. The remaining task is to show (20) is satisfied by induction. For $k = 1$,

$$\begin{aligned} \|\mathbf{X}_1 - \mathbf{P}\|_F &\leq \|\mathbf{X}_1 - \mathbf{A}\|_F + \|\mathbf{A} - \mathbf{P}\|_F \leq l + \frac{r}{2} \\ &\leq 2r + \frac{s}{4} \leq \frac{s(1-\epsilon)}{2(2+\epsilon)} + \frac{s}{4} < s. \end{aligned}$$

Assume that (20) is satisfied when $n = k$, then it follows from (19) that

$$\|\mathbf{X}_k - \pi(\mathbf{X}_k)\|_F \leq c^k \|\mathbf{X}_1 - \pi(\mathbf{X}_1)\|_F \leq 2lc^k. \quad (21)$$

For an arbitrary k and $i = 1$ or 2 , we have

$$\begin{aligned} &\|\mathbf{X}_{k-2} - \pi(\mathbf{X}_{k-1})\|_F \\ &= \|\mathbf{X}_{k-2} - \pi(\pi_i(\mathbf{X}_{k-2}))\|_F \\ &= \|\mathbf{X}_{k-2} - \pi(\mathbf{X}_{k-2}) + \pi(\mathbf{X}_{k-2}) - \pi(\pi_i(\mathbf{X}_{k-2}))\|_F \\ &\leq \|\mathbf{X}_{k-2} - \pi(\mathbf{X}_{k-2})\|_F + \|\pi(\mathbf{X}_{k-2}) - \pi(\pi_i(\mathbf{X}_{k-2}))\|_F \\ &\leq \|\mathbf{X}_{k-2} - \pi(\mathbf{X}_{k-2})\|_F + \alpha \|\mathbf{X}_{k-2} - \pi_i(\mathbf{X}_{k-2})\|_F \\ &\leq (1 + \alpha) \|\mathbf{X}_{k-2} - \pi(\mathbf{X}_{k-2})\|_F. \end{aligned}$$

The second part of the second inequality follows by the continuous of π , the third inequality follows by

$$\|\mathbf{X}_{k-2} - \pi_i(\mathbf{X}_{k-2})\|_F \leq \|\mathbf{X}_{k-2} - \pi(\mathbf{X}_{k-2})\|_F, \quad i = 1, 2.$$

In addition, when k is even, by lemma 3.2, we have

$$\|\pi(\mathbf{X}_k) - \pi(\mathbf{X}_{k-1})\|_F < \varepsilon(\epsilon) \|\mathbf{X}_{k-1} - \pi(\mathbf{X}_{k-1})\|_F. \quad (22)$$

When k is odd, applying Lemma 3.6 gives

$$\begin{aligned} &\|\pi(\mathbf{X}_k) - \pi(\mathbf{X}_{k-1})\|_F \\ &< \varepsilon_1(\epsilon) \|\mathbf{X}_{k-1} - \pi(\mathbf{X}_{k-1})\|_F + \varepsilon_2(\epsilon) \|\mathbf{X}_{k-2} - \pi(\mathbf{X}_{k-1})\|_F \\ &< \varepsilon_1(\epsilon) \|\mathbf{X}_{k-1} - \pi(\mathbf{X}_{k-1})\|_F \\ &\quad + \varepsilon_2(\epsilon)(1 + \alpha) \|\mathbf{X}_{k-2} - \pi(\mathbf{X}_{k-2})\|_F \\ &\leq 2\varepsilon_1(\epsilon)c^{k-1}l + 2\varepsilon_2(\epsilon)(1 + \alpha)c^{k-2}l \\ &= (\varepsilon_1(\epsilon)c + \varepsilon_2(\epsilon)(1 + \alpha))2c^{k-2}l. \end{aligned}$$

Set $\varepsilon = \max\{\varepsilon(\epsilon), \varepsilon_1(\epsilon)\}$, then for an arbitrary k , we have

$$\|\pi(\mathbf{X}_k) - \pi(\mathbf{X}_{k-1})\|_F \leq (\varepsilon c + \varepsilon_2(\epsilon)(1 + \alpha))2c^{k-2}l. \quad (23)$$

By combining (23) and using Lemma 3.2, we obtain

$$\begin{aligned} &\|\pi(\mathbf{X}_k) - \pi(\mathbf{A})\|_F \\ &\leq \|\pi(\mathbf{A}) - \pi(\mathbf{X}_1)\|_F + \|\pi(\mathbf{X}_2) - \pi(\mathbf{X}_1)\|_F \\ &\quad + \left\| \sum_{j=3}^k \pi(\mathbf{X}_j) - \pi(\mathbf{X}_{j-1}) \right\|_F \\ &\leq \varepsilon l + 2\varepsilon l + \sum_{j=3}^k (\varepsilon_1(\epsilon)c + \varepsilon_2(\epsilon)(1 + \alpha))2c^{j-2}l \\ &\leq 3\varepsilon l + \frac{2(\varepsilon_1(\epsilon)c + \varepsilon_2(\epsilon)(1 + \alpha))}{1 - c} l \\ &= \frac{3\varepsilon(1 - c) + 2\varepsilon c + (1 + \alpha)\varepsilon_2(\epsilon)}{1 - c} l \leq \epsilon l. \end{aligned} \quad (24)$$

Thus,

$$\begin{aligned} \|\mathbf{P} - \mathbf{X}_k\|_F &\leq \|\mathbf{P} - \pi(\mathbf{A})\|_F + \|\pi(\mathbf{A}) - \pi(\mathbf{X}_k)\|_F \\ &\quad + \|\pi(\mathbf{X}_k) - \mathbf{X}_k\|_F \leq s/4 + \epsilon l + 2l < s, \end{aligned}$$

which shows that (20) is satisfied.

It follows from (23) that the sequence $(\pi(\mathbf{X}_k))_{k=1}^\infty$ is a Cauchy sequence which converges to a point \mathbf{Z}_∞ . Note that (21) is satisfied, the sequence $(\mathbf{X}_k)_{k=1}^\infty$ also converges. In addition, $\mathbf{Z}_\infty = \pi(\mathbf{Z}_\infty)$ can be derive by noting that the projection is local continuous. Moreover, by taking the limit of (24) we can get (i). For (ii). Note that

$$\begin{aligned} \|\pi(\mathbf{X}_k) - \mathbf{X}_\infty\|_F &\leq \sum_{j=k+1}^\infty \|\pi(\mathbf{X}_j) - \pi(\mathbf{X}_{j-1})\|_F \\ &\leq \frac{2l\varepsilon c^k}{1 - c} + \frac{2(1 + \alpha)l\varepsilon_2(\epsilon)c^{k-1}}{1 - c}, \end{aligned}$$

and combine with (21), we can get

$$\begin{aligned} \|\mathbf{X}_k - \mathbf{X}_\infty\|_F &\leq \|\mathbf{X}_k - \pi(\mathbf{X}_k)\|_F + \|\pi(\mathbf{X}_k) - \mathbf{X}_\infty\|_F \\ &\leq \left(2l + \frac{2l\varepsilon}{1 - c} + \frac{2(1 + \alpha)l\varepsilon_2(\epsilon)}{1 - c} \right) c^k \\ &= \beta c^k l, \end{aligned}$$

with a constant β as desired.

4 EXPERIMENTAL RESULTS

The main aim of this section is to demonstrate that (i) the computational time required by the proposed TAP method is faster than that by the original alternating projection (AP) method with about the same approximation; (ii) the performance of the proposed TAP method is better than that of nonnegative matrix factorization methods in terms of computational time and accuracy for examples in data clustering, pattern recognition and hyperspectral data analysis.

The experiments in Subsection 4.1 are performed under Windows 7 and MATLAB R2018a running on a desktop (Intel Core i7, @ 3.40GHz, 8.00G RAM) and experiments in Subsections 4.2-4.5 are performed under Windows 10 and MATLAB R2020a running on a desktop (AMD Ryzen 9 3950, @ 3.49GHz, 64.00G RAM).

4.1 The First Experiment

In the first experiment, we randomly generated n -by- n nonnegative matrices \mathbf{A} where their matrix entries follow a uniform distribution in between 0 and 1. We employed the proposed TAP method and the original alternating projection (AP) method [34] to test the relative approximation error $\|\mathbf{A} - \mathbf{X}_c\|_F / \|\mathbf{A}\|_F$, where \mathbf{X}_c are the computed rank r solutions by different methods. For comparison, we also list the results by nonnegative matrix factorization algorithms: A-MU [25], A-HALS [25] and A-PG [29].

Tables 1 shows the relative approximation error of the computed solutions from the proposed TAP method and the other testing methods for synthetic data sets of sizes 200-by-200, 400-by-400 and 800-by-800. Note that there is no guarantee that other testing NMF algorithms can determine the underlying nonnegative low rank factorization. In the tables, it is clear that the testing NMF algorithms cannot obtain the underlying low rank factorization. One of the reason may be that NMF algorithms can be sensitive to initial guesses. In the tables, we illustrate this phenomena by displaying the mean relative approximation error and the range containing both the minimum and the maximum

TABLE 1

The relative approximation error and computation time on the synthetic data sets. The **best** values are respectively highlighted by bolder fonts.

200-by-200 matrix						
Method	Relative approximation error			Computation time		
	$r = 10$	$r = 20$	$r = 40$	$r = 10$	$r = 20$	$r = 40$
TAP	0.4576	0.4161	0.3247	0.42	0.48	0.38
AP	0.4576	0.4161	0.3247	0.66	0.66	0.42
A-MU:mean	0.4592	0.4249	0.3733	8.32	9.54	15.34
A-MU:range	[0.4591, 0.4593]	[0.4246, 0.4251]	[0.3729, 0.3737]	[8.00, 8.81]	[9.41, 9.61]	[14.72, 15.75]
A-HALS:mean	0.4591	0.4246	0.3717	1.09	1.95	4.01
A-HALS:range	[0.4590, 0.4593]	[0.4244, 0.4247]	[0.3714, 0.3719]	[0.98, 1.22]	[1.86, 2.05]	[3.86, 4.13]
A-PG:mean	0.4591	0.4244	0.3717	14.77	16.24	21.52
A-PG:range	[0.4590, 0.4592]	[0.4243, 0.4246]	[0.3715, 0.3719]	[14.50, 15.03]	[15.81, 16.55]	[21.02, 21.77]
400-by-400 matrix						
Method	Relative approximation error			Computation time		
	$r = 20$	$r = 40$	$r = 80$	$r = 20$	$r = 40$	$r = 80$
TAP	0.4573	0.4161	0.3421	1.55	1.32	1.10
AP	0.4573	0.4161	0.3421	2.95	2.47	1.68
A-MU:mean	0.4606	0.4301	0.3857	37.80	38.72	46.41
A-MU:range	[0.4605, 0.4607]	[0.4300, 0.4302]	[0.3856, 0.3860]	[36.67, 39.03]	[38.21, 39.18]	[45.87, 48.28]
A-HALS:mean	0.4604	0.4295	0.3836	3.10	7.40	19.67
A-HALS:range	[0.4603, 0.4605]	[0.4294, 0.4296]	[0.3833, 0.3838]	[3.03, 3.25]	[7.12, 7.60]	[19.04, 20.61]
A-PG:mean	0.4604	0.4297	0.3850	51.68	60.80	61.95
A-PG:range	[0.4604, 0.4605]	[0.4296, 0.4298]	[0.3847, 0.3853]	[51.04, 52.26]	[60.62, 61.01]	[61.34, 62.64]
800-by-800 matrix						
Method	Relative approximation error			Computation time		
	$r = 40$	$r = 80$	$r = 160$	$r = 40$	$r = 80$	$r = 160$
TAP	0.4550	0.4144	0.3412	7.14	4.84	4.80
AP	0.4550	0.4144	0.3412	15.84	9.55	7.11
A-MU:mean	0.4608	0.4350	0.3984	60.29	60.96	61.31
A-MU:range	[0.4607, 0.4609]	[0.4349, 0.4351]	[0.3982, 0.3986]	[60.03, 60.65]	[60.61, 61.58]	[60.72, 61.94]
A-HALS:mean	0.4605	0.4336	0.3984	18.54	47.70	61.30
A-HALS:range	[0.4604, 0.4605]	[0.4335, 0.4336]	[0.3982, 0.3986]	[17.76, 19.48]	[43.33, 52.75]	[60.71, 61.91]
A-PG:mean	0.4606	0.4343	0.4007	60.38	61.26	61.76
A-PG:range	[0.4606, 0.4607]	[0.4342, 0.4344]	[0.4005, 0.4012]	[60.12, 60.79]	[60.78, 61.81]	[61.29, 62.48]

relative approximation errors by using ten initial guesses randomly generated. We find in the table that the relative approximation errors computed by the TAP method is the same as those by the AP method. It implies that the proposed TAP method can achieve the same accuracy of classical alternating projection. According to the tables, the relative approximation errors by both TAP and AP methods are always smaller than the minimum relative approximation errors by the testing NMF algorithms. In addition, we report the computational time (seconds calculated by MATLAB) in the tables. We see that the computational time required by the proposed TAP method is less than that required by AP method.

4.2 The Second Experiment

4.2.1 Face Data

In this subsection, we consider two frequently-used face data sets, i.e., the ORL face data set¹ and the Yale B face

data set². The ORL face data set contains images from 40 individuals, each providing 10 different images with the size 112×92 . In the Yale B face data set, we take a subset which consists of 38 people and 64 facial images with different illuminations for each individual. Each testing image is reshaped to a vector, and all the image vectors are combined together to form a nonnegative matrix. Here we perform NMF algorithms and TAP algorithm to obtain low rank approximations with a predefined rank r . There are several NMF algorithms to be compared, namely multiplicative updates (MU) [8], [30], accelerated MU (A-MU) [25], hierarchical alternating least squares (HALS) algorithm [23], accelerated HALS (A-HALS) [25], projected gradient (PG) Method [29], and accelerated PG (A-PG) [29].

Firstly, we compare the low rank approximation results by different methods with respect to different predefined ranks r . We report the relative approximation errors in Table 2. For ORL data set, we set r to be 10 and 40 because face data contains 40 individuals and each individual has 10

1. <http://www.uk.research.att.com/facedatabase.html>

2. <http://vision.ucsd.edu/~leekc/ExtYaleDatabase/ExtYaleB.html>

TABLE 2

The relative approximation error on the Yale-B data set and the ORL data set. The **best** values and the **second best** values are respectively highlighted by bolder fonts and underlines.

Dataset	Rank	MU	A-MU	HALS	A-HALS	PG	A-PG	AP	TAP
Yale B	$r = 38$	0.186	0.182	<u>0.181</u>	<u>0.181</u>	0.187	0.184	0.166	0.166
	$r = 64$	0.160	0.157	<u>0.152</u>	<u>0.152</u>	0.159	0.159	0.133	0.133
ORL	$r = 10$	0.206	0.206	<u>0.205</u>	<u>0.205</u>	0.206	0.206	0.204	0.204
	$r = 40$	0.159	0.156	<u>0.155</u>	<u>0.155</u>	0.160	0.158	0.147	0.147

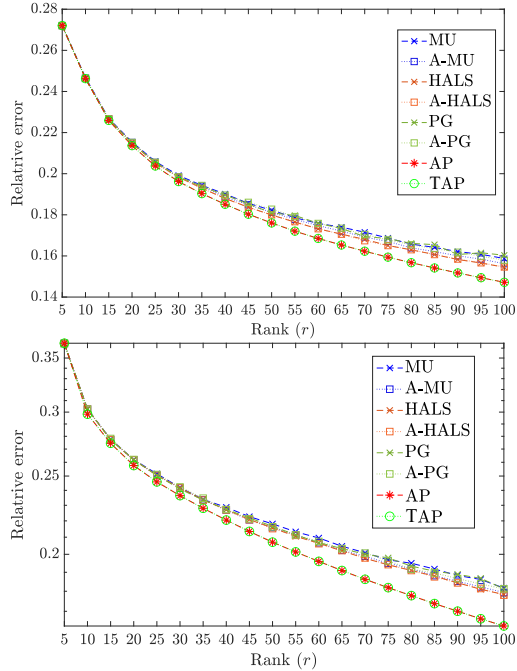


Fig. 3. Relative approximation errors on the ORL data set (Top) and the Yale B data set (Bottom), with respect to the different ranks r .

different images. Similarly, r is set to be 38 and 64 for Yale B data set. In the numerical results, we compare the relative approximation error: $\|\mathbf{X}_c - \mathbf{A}\|_F / \|\mathbf{A}\|_F$. For the TAP and AP methods the nonnegative low rank approximation is directly computed, while for the NMF methods, we multiply the factor matrices. We can see from the table that the relative approximation errors by TAP and AP methods are lower than those by NMF methods.

The relative approximation errors on these two face data sets with respect to different ranks r are plotted in Figure 3. We can see that as r increases, the gap of relative approximation errors between TAP (or AP) method and NMF methods becomes larger. The total computational time required by the proposed TAP method (2.84 seconds) is less than that (17.44 seconds) required by the AP method. The proposed TAP method is more efficient than the AP method.

Next, we test the face recognition performance with respect to TAP approximations and NMF approximations. We use the k -fold cross-validation strategy. For each data set, the data is split into k ($k = 10$ for the ORL data set and $k = 64$ for the Yale B data set) groups and each group contains one facial image of each individual. For instance, the ORL data set is split into $k = 10$ groups and each group contains 40 facial images. Then, we circularly take one group

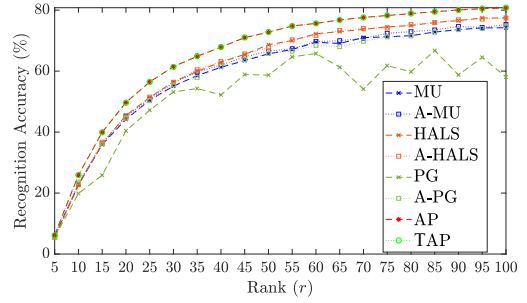


Fig. 4. The recognition accuracy (%) on Yale-B dataset with respect to rank r .

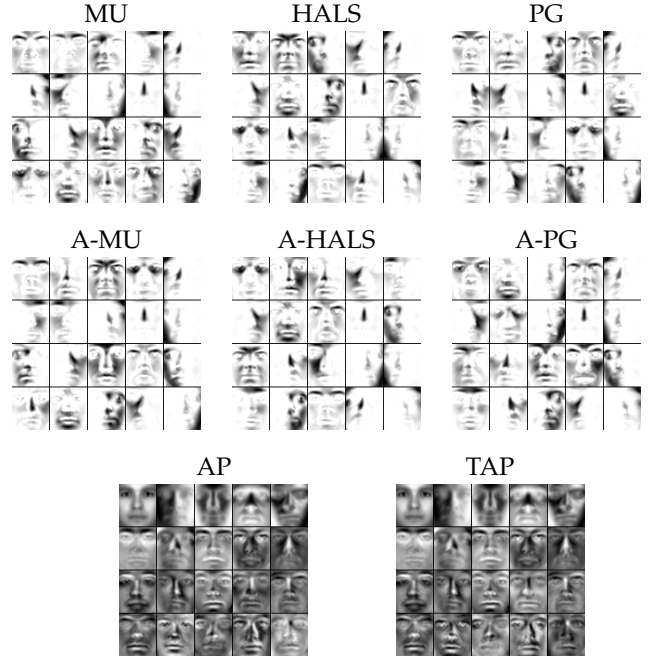


Fig. 5. The first 20 singular vectors of the results by TAP (or AP) method and the columns of left factor matrices resulted by NMF methods when the rank $r = 20$. These vectors are reshaped to the size of facial images and their values are adaptively normalized.

as a test data set and the remaining groups as a training data set until all the groups have been selected as the test data. Given the original training data $\mathbf{A}_{\text{train}}$ with the size $m \times n$, where n indicates the pixels of each face image and m is the amount of training samples, we first perform NMF and TAP (or AP) algorithms to obtain non-negative low rank approximations $\mathbf{A}_{\text{train}} \approx \mathbf{B}_{\text{NMFtrain}} \mathbf{C}_{\text{NMFtrain}}$ and $\mathbf{A}_{\text{train}} \approx \mathbf{U}_{\text{TAPtrain}} \mathbf{\Sigma}_{\text{TAPtrain}} \mathbf{V}_{\text{TAPtrain}}$ respectively with rank r . The new representations of $\mathbf{A}_{\text{train}}$ are given by $\mathbf{U}_{\text{NMFtrain}}^T \mathbf{A}_{\text{train}}$ and $\mathbf{U}_{\text{TAPtrain}}^T \mathbf{A}_{\text{train}}$ respectively by the NMF methods and the TAP (or AP) method. The nearest neighbor (NN) classifier is adopted by recognized the testing data based on the distance between their representations and the projected training data.

The face recognition results are exhibited in Table 3. From this table, we can see that the accuracies based on TAP approximations are higher than those based on NMF approximations. To further investigate how the rank r affects the recognition results, we plot the recognition accuracy on Yale B data set with respect to r in Figure 4. It can be found that the recognition accuracy based on TAP and AP approx-

TABLE 3

The recognition accuracy on the Yale-B dataset and ORL dataset. The **best** values and the second best values are respectively highlighted by bolder fonts and underlines.

Dataset	Parameter	MU	A-MU	HALS	A-HALS	PG	A-PG	AP	TAP
Yale B	$r = 38$	61.061%	61.143%	61.637%	62.253%	58.306%	60.074%	66.776%	67.681%
	$r = 64$	69.942%	70.477%	72.821%	72.821%	65.502%	68.586%	<u>76.563%</u>	76.809%
ORL	$r = 10$	95.750%	96.250%	96.250%	96.250%	96.500%	96.500%	96.750%	96.750%
	$r = 40$	<u>98.250%</u>	98.000%	<u>98.250%</u>	98.500%	79.250%	<u>98.250%</u>	98.500%	98.500%

TABLE 4

The accuracy and NMI values of the document clustering results on the TDT2 data set.

Metric	MU	A-MU	HALS	A-HALS	PG	A-PG	AP	TAP
Accuracy	52.800%	50.724%	54.322%	53.108%	54.205%	51.661%	<u>61.294%</u>	61.326%
NMI	0.674	0.651	0.663	0.643	<u>0.681</u>	0.661	0.728	0.728

imations is always better than those based on NMF approximations. Meanwhile, to see the features learned by different methods, we exhibit the column vectors of $\mathbf{B}_{\text{NMFtrain}}$ and singular vectors of $\mathbf{U}_{\text{TAPtrain}}$ in Figure 5. These vectors are reshaped to the same size as facial images and their values are normalized to $[0, 255]$ for the display purpose. We see that the nonnegative low rank matrix approximation methods do not give the part-based representations, but provides different important facial representations in the recognition.

4.2.2 Document Data

In this subsection, we use the NIST Topic Detection and Tracking (TDT2) corpus as the document data. The TDT2 corpus consists of data collected during the first half of 1998 and taken from 6 sources, including 2 newswires (APW, NYT), 2 radio programs (VOA, PRI) and 2 television programs (CNN, ABC). It consists of 11201 on-topic documents which are classified into 96 semantic categories. In this experiment, the documents appearing in two or more categories were removed, and only the largest 30 categories were kept, thus leaving us with 9394 documents in total. Then, each document is represented by the weighted term-frequency vector [16], and all the documents are gathered as a matrix \mathbf{A}_{doc} of size 9394×36771 . By using the procedure given in [16], we compute the projected results $\mathbf{U}_{\text{TAP}}^T \mathbf{A}_{\text{TAP}} = \mathbf{\Sigma}_{\text{TAP}} \mathbf{V}_{\text{TAP}}^T$, and then use k -means clustering method and Kuhn-Munkres algorithm to find the best mapping which maps each cluster label to the equivalent label from the document corpus. For NMF methods, we scale each column of \mathbf{B}_{NMF} such that their ℓ_2 norms are equal to 1, and the corresponding scaled \mathbf{C}_{NMF} is used for clustering and label assignment. To quantitatively evaluate the clustering performance of each method, we selected two metrics, i.e., the accuracy and the normalized mutual information (NMI) (we refer to [38] for detailed discussion). According to Table (4), it is clear that nonnegative low rank matrix approximation can provide more effective latent features ($\mathbf{U}_{\text{TAP}}^T \mathbf{A}_{\text{TAP}} = \mathbf{\Sigma}_{\text{TAP}} \mathbf{V}_{\text{TAP}}^T$) for document clustering task. Note that the computational time required by the proposed TAP method (309.22 seconds) is less than that (3417.33 seconds) required by the AP method. Again the results demonstrate that the proposed TAP method is more efficient than the AP method.

4.3 Separable Nonnegative Matrices

In this subsection, we compare the performance of the nonnegative low rank matrix approximation method and separable NMF algorithms. Here we generate two kinds of synthetic separable nonnegative matrices.

- (Separable) The first case $\mathbf{A} = \mathbf{BC} + \mathbf{N}$ is generated the same as [26], in which $\mathbf{B} \in \mathbb{R}^{200 \times 20}$ is *uniform distributed* and $\mathbf{C} = [\mathbf{I}_{20}, \mathbf{H}'] \in \mathbb{R}^{20 \times 210}$ with \mathbf{H}' containing all possible combinations of two non-zero entries equal to 0.5 at different positions. The columns of \mathbf{BH}' are all the middle points of the columns of \mathbf{B} . Meanwhile, the i -th column of \mathbf{N} , denoted as n_i , obeys $n_i = \sigma(m_i - \bar{w})$ for $21 \leq i \leq 210$, where $\sigma > 0$ is the noise level, m_i is the i -th column of \mathbf{B} , and \bar{w} denotes the average of columns of \mathbf{B} . This means that we move the columns of \mathbf{A} toward the outside of the convex hull of the columns of \mathbf{B} .
- (Generalized separable) The second case is generated almost the same as the first case but simultaneously considering the separability of rows, known as generalized separable NMF [31]. For this case, the size of \mathbf{A} is set as 78×55 with column-rank 10 and row-rank 12, being the same as [31].

Firstly, we test the approximation ability of TAP and AP methods, NMF methods, and the successive projection algorithm (SPA) [26], [39] for separable NMF for synthetic separable data. For the generalized separable case, we compare the TAP (or AP) method with SPA, the generalized SPA (GSPA) [31], and the generalized separable NMF with a fast gradient method (GS-FGM) [31]. Note that when we apply SPA on the generalized separable matrix, we run it firstly to identify the important columns and with the transpose of the input to identify the important rows. This variant is referred to SPA*. The noise level σ is logarithmic spaced in the interval $[10^{-3}, 1]$. For each noise level, we independently generate 25 matrices for both separable and generalized separable cases, respectively. We report the averaged approximation error in Figures 6 and 7. It can be found that TAP and AP methods can achieve the lowest average errors in the testing examples.

The approximation errors of TAP and AP methods are much lower than separable and generalized separable NMF

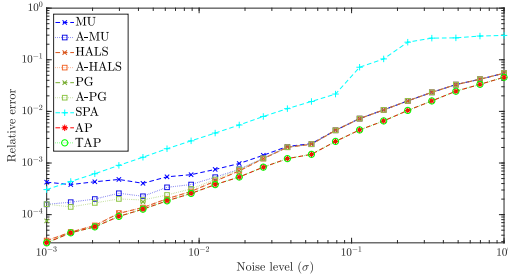


Fig. 6. Average relative approximation error on separable matrices (Case 1), with respect to the different values of σ .

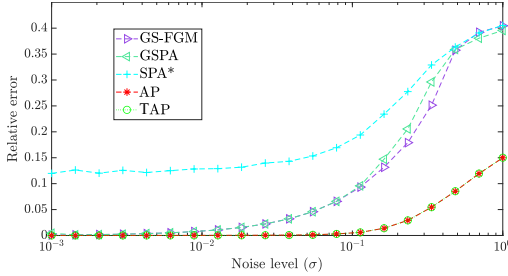


Fig. 7. Average relative approximation error on generalized separable matrices (Case 2), with respect to the different values of σ .

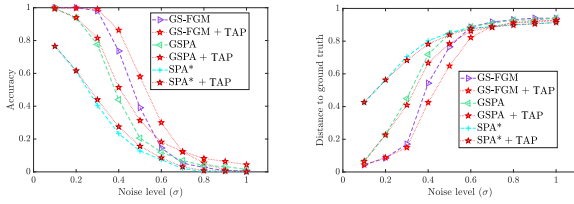


Fig. 8. Average accuracy (left) and distance to ground truth (right) for the different algorithms on generalized separable matrices (Case 2), with respect to the different σ s.

methods when the noise level is high. Note that the average computational time required by the proposed TAP method (0.0064 seconds) is less than that (0.0165 seconds) required by the AP method. It is interesting whether a better nonnegative low rank matrix approximation could contribute to a better separable (or generalized separable) NMF result. To further investigate whether nonnegative low rank matrix approximation could help separable and generalized separable NMF methods, we conduct the experiments with inputting the nonnegative low rank approximation to separable and generalized separable NMF methods. We adopt the accuracy and the distance to ground truth defined in Eqs. (16) and (17) of [31] as the quantitative metrics. The accuracy reports the proportion of correctly identified row and column indices while the distance to ground truth reports the relative errors between the identified important rows (columns) to the ground truth important rows (columns). We present the computational results in Figure 8. When the noise level is between 0.1 and 1, the nonnegative low rank matrix approximation by our TAP method obviously enhances the accuracy and decrease the distance between the identified rows (columns) to the ground truth.

4.4 Symmetric Nonnegative Matrices for Graph Clustering

In this subsection, we test TAP and AP methods on the symmetric matrices. It can readily be found that the output of TAP and AP algorithms would be symmetric if the input matrix is symmetric since that the projection onto the nonnegative matrix manifold or the low rank matrix manifold would never affect the symmetry. Here symmetric NMF methods are the coordinate descent algorithm (denoted as “CD-symNMF”) [40], the Newton-like algorithm (denoted as “Newton-symNMF”) [27], and the alternating least squares algorithm (denoted as “ALS-symNMF”) [27].

We perform experiments by using symmetric NMF methods, TAP and AP methods on the synthetic graph data, which is reproduced from [41] with six different cases. The data points in 2-dimensional space are displayed in the first row of Figure 9. Each case contains clear cluster structures. By following the procedures in [27], [41], a similarity matrix $\mathbf{A} \in \mathbb{R}^{n \times n}$, where n represents the number of data points, is constructed to characterize the similarity between each pair of data points. Each data point is assumed to be only connected to its nearest nine neighbors. Given a specific pair of the i -th and j -th data points x_i and x_j , we firstly construct the distance matrix $\mathbf{D} \in \mathbb{R}^{n \times n}$ with $D_{ij} = D_{ji} = \|x_i - x_j\|_2^2$. Then, the similarity matrix is given as

$$A_{ij} = \begin{cases} 0, & \text{if } i = j, \\ e^{\frac{-D_{ij}}{\sigma_i \sigma_j}}, & \text{if } i \neq j, \end{cases} \quad (25)$$

where σ_i is the Euclidean distance between the i -th data point x_i and its 9-th neighbor. Then, we perform NMF, TAP and AP methods for \mathbf{A} .

The clustering results of the symmetric NMF methods and nonnegative low rank matrix approximation are obtained by using k -means method on \mathbf{B} and \mathbf{U} respectively. The clustering results are shown in Figure 9. CD-symNMF method fails in most examples except the example in the second column. Both Newton-symNMF and ALS-symNMF methods fail in the example in the fifth column. However, TAP and AP methods perform well for all the examples. The average computational time required by the proposed TAP method (0.0321 seconds) is less than that (0.1035 seconds) required by the AP method. The proposed TAP is faster than the AP method.

4.5 Orthogonal Decomposable Non-negative Matrices

In this subsection, we test TAP and AP methods and orthogonal NMF (ONMF) methods [4], [24] on the approximation of the synthetic data and the unmixing of hyperspectral images. The orthogonal NMF method is a multiplicative updating algorithm proposed by Ding et al. [4]. We refer to Ding-Ti-Peng-Park (DTPP)-ONMF. A multiplicative updating algorithm utilizing the true gradient in Stiefel manifold is proposed in [24]. We refer to SM-ONMF.

We construct an orthogonal nonnegative matrix $\mathbf{B} \in \mathbb{R}^{100 \times 10}$, whose transpose is shown in Figure 10. Then a matrix $\mathbf{C} \in \mathbb{R}^{10 \times 30}$ is generated with entries uniformly distributed in $[0, 1]$. Then, we obtain an orthogonal decomposable matrix $\mathbf{A} = \mathbf{BC} \in \mathbb{R}^{100 \times 30}$. Next, a noise matrix based on MATLAB command $\sigma \times \text{rand}(100, 30)$ is

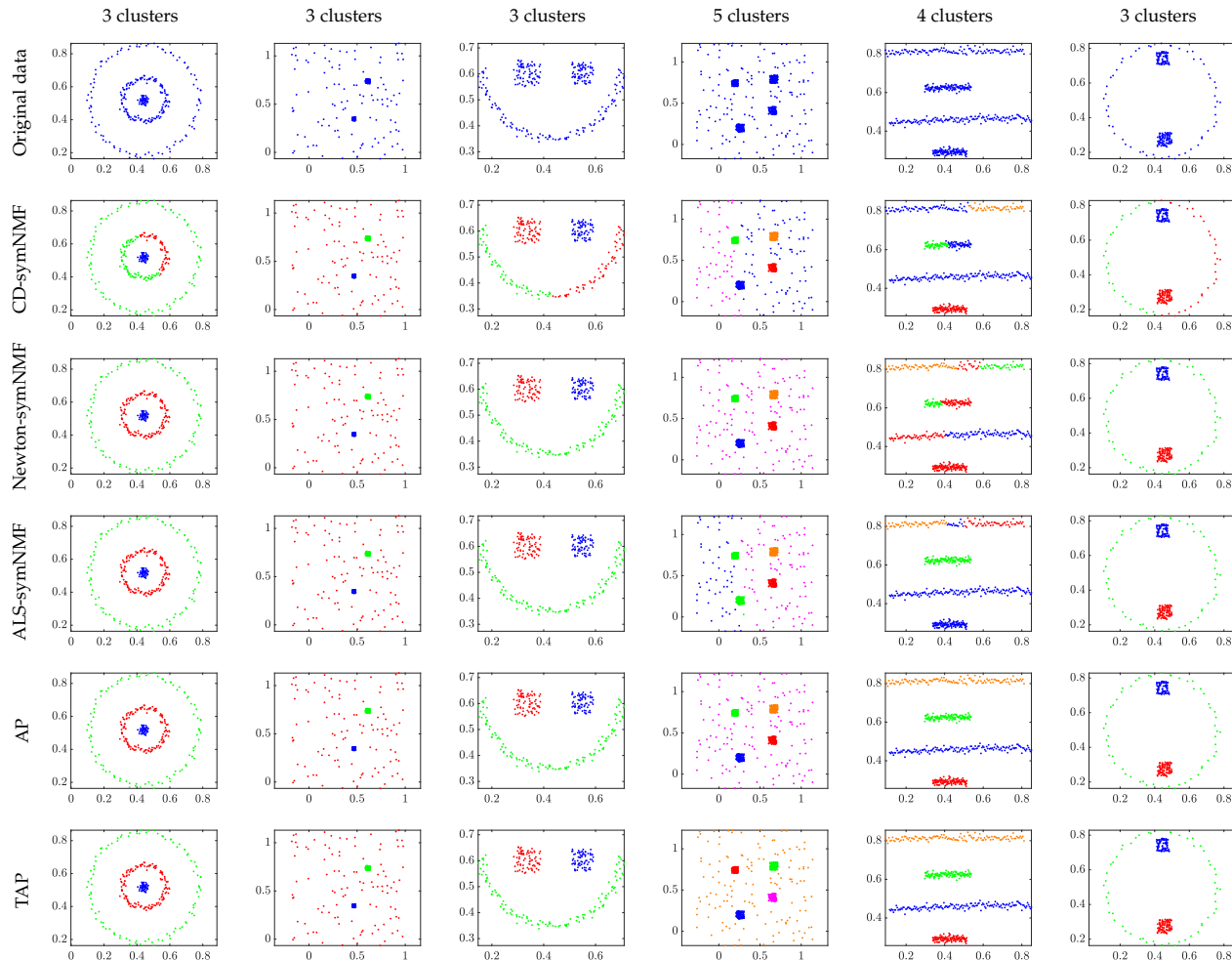


Fig. 9. The graph clustering results by the TAP (or AP) method and symmetric NMF methods on 6 cases of synthetic graph data. Different color represents different clusters.

added to \mathbf{A} . We set $\sigma = 0, 0.02, 0.04, \dots, 0.1$. The relative approximation errors of the results by different methods are shown in Table 5. We can see that the approximation errors of TAP and AP methods are the lowest among the testing examples.

As a real-world application of ONMF, hyperspectral image unmixing aims at factoring the observed hyperspectral image in matrix format into an endmember matrix and an abundance matrix. The abundance matrix is indeed the classification of the pixels to different clusters, with each corresponding to a material (endmember). In this part, we use a sub-image of the Samson data set [42], consisting of $95 \times 95 = 9025$ spatial pixels and 156 spectral bands. We form a matrix \mathbf{A} of size 9025×156 to represent this sub-image. Three different materials, i.e., “Tree”, “Rock”, and “Water”, are in this sub-image, and we set the rank r as 3. The factor matrices $\mathbf{B} \in \mathbb{R}^{9025 \times 3}$ and $\mathbf{C} \in \mathbb{R}^{3 \times 156}$ can be obtained by the orthogonal NMF methods. We use k-means and do hard clustering on $\mathbf{B} \in \mathbb{R}^{9025 \times 3}$ to obtain the abundance matrix, and we can obtain the i -th feature image by reshaping its i -th column to a 95×95 matrix. Each row of \mathbf{C} represents the spectral reflectance of on material (“Tree”, “Rock”, or “Water”). As for TAP and AP methods, we apply singular value decomposition on approximated non-

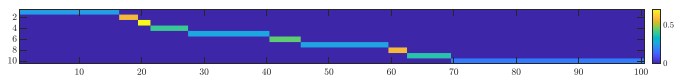


Fig. 10. An illustration of the generated \mathbf{B}^T .

TABLE 5
The relative approximation errors ($\times 100$) on the orthogonal symmetric matrix data. The **best** values and the second best values are respectively highlighted by bolder fonts and underlines.

σ	0	0.02	0.04	0.06	0.08	0.1
DTPP-ONMF	0.022	<u>2.730</u>	5.231	7.567	9.465	<u>11.232</u>
SM-ONMF	0.016	2.741	5.169	7.533	9.424	14.180
AP	0.000	2.364	4.471	6.529	8.215	9.700
TAP	0.000	2.364	4.471	6.529	8.215	9.700

negative low rank matrices to obtain the left singular value matrices which contain the first 3 left singular vectors. Then, we use k-means and do hard clustering on the left singular matrices to cluster three materials and obtain abundance matrices and endmember matrices.

To quantitatively evaluate the unmixing results, we employ two metrics. The first one is the spectral angle distance

TABLE 6

The quantitative metrics of the unmixing results on the hyperspectral image Samson. The **best** values and the second best values are respectively highlighted by bolder fonts and underlines.

Metric	DTPP-ONMF	SM-ONMF	AP	TAP
SAD	<u>0.3490</u>	0.4389	0.0765	0.0765
Similarity	<u>0.5887</u>	0.5640	0.9383	0.9383

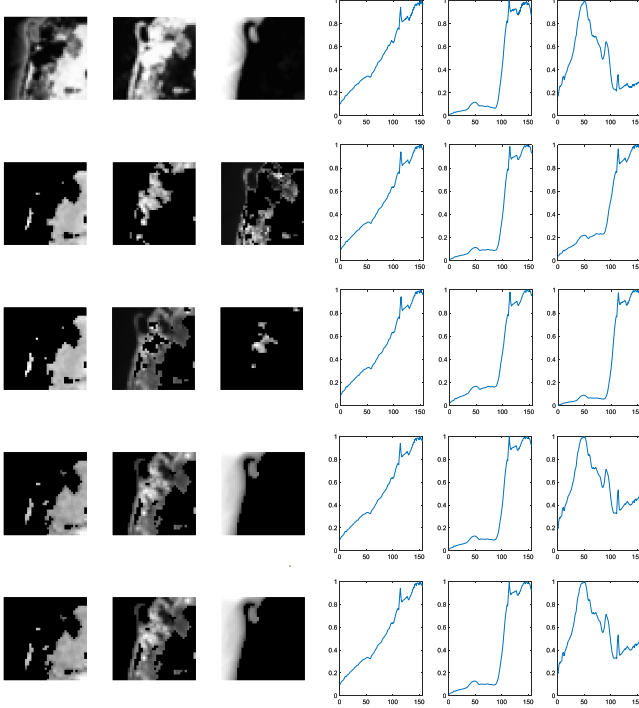


Fig. 11. Left: Rock, Tree, Water; Right: Reflectance of Rock, Tree, Water. From the top to bottom: groundtruth, DTPP-ONMF, SM-ONMF, AP, TAP.

(SAD) as follows:

$$\text{SAD} = \frac{1}{r} \sum_{i=1}^r \arccos \left(\frac{s_i^T \hat{s}_i}{\|s_i\|_2 \|\hat{s}_i\|_2} \right),$$

where $\{s_i\}_{i=1}^r$ are the estimated spectral reflectance (rows of the endmember matrix) and $\{\hat{s}_i\}_{i=1}^r$ are the groundtruth spectral reflectance. The second one is the similarity of the abundance feature image [43] as follows:

$$\text{Similarity} = \frac{1}{r} \sum_{i=1}^r \frac{a_i^T \hat{a}_i}{\|a_i\|_2 \|\hat{a}_i\|_2},$$

where $\{a_i\}_{i=1}^r$ are the estimated abundance feature (columns of the abundance matrix) and $\{\hat{a}_i\}_{i=1}^r$ are the groundtruth ones. We note that a larger Similarity and a smaller SAD indicate a better unmixing result. We exhibit the quantitative metrics in Table 6. We can evidently see that the proposed TAP and AP methods obtain the best metrics. Meanwhile, we illustrate the estimated spectral reflectance and abundance feature images in Figure 6. It can be found from the second row that DTPP-ONMF and SM-ONMF perform well for the materials ‘‘Rock’’ and ‘‘Tree’’ but poor on ‘‘Water’’. TAP and AP methods unmix these three materials well, but the proposed TAP method (the

computational time = 0.1492 seconds) is faster than the AP method (the computational time = 0.3738 seconds).

5 CONCLUSION

In this paper, we have proposed a new alternating projection method to compute nonnegative low rank matrix approximation for nonnegative matrices. Our main idea is to use the tangent space of the point in the fixed-rank matrix manifold to approximate the projection onto the manifold in order to reduce the computational cost. Numerical examples in data clustering, pattern recognition and hyperspectral data analysis have shown that the proposed alternating projection method is better than that of nonnegative matrix factorization methods in terms of accuracy, and the computational time required by the proposed alternating projection method is less than that required by the original alternating projection method.

Moreover, we have shown that the sequence generated by the alternating projections onto the tangent spaces of the fixed rank matrices manifold and the nonnegative matrix manifold, converge linearly to a point in the intersection of the two manifolds where the convergent point is sufficiently close to optimal solutions. Our theoretical convergence results are new and are not studied in the literature. We remark that Andersson and Carlsson [37] assumed that the exact projection onto each manifold and then obtained the convergence result of the alternating projection method. Because of our proposed inexact projection onto each manifold, our proof can be extended to show the sequence generated by alternating projections on one or two nontangential manifolds based on tangent spaces, converges linearly to a point in the intersection of the two manifolds.

As a future research work, it is interesting to study (i) the convergence results when inexact projections on several manifolds are employed, and (ii) applications where the other norms (such as l_1 norm) in data fitting instead of Frobenius norm. It is necessary to develop the related algorithms for such manifold optimization problems.

APPENDIX A

PROOF OF LEMMA 3.4, 3.6 AND 3.7

A.1 Proof of Lemma 3.4

Proof. For a given $\epsilon > 0$, there exist an $s_1(\epsilon)$ such that Lemma 3.3 applies to $\mathcal{M}_r \cap \text{Ball}(\mathbf{P}, s_1(\epsilon))$. Since $\pi_1(\cdot)$ and $P_{T_{\mathcal{M}_r}(\cdot)}(\cdot)$ are continuous, there exist an $s(\epsilon) < s_1(\epsilon)$ such that the image of $\text{Ball}(\mathbf{P}, s(\epsilon))$ under π_1 and $P_{T_{\mathcal{M}_r}(\cdot)}$ is included in $\text{Ball}(\mathbf{P}, s_1(\epsilon))$. Now we can choose a point $\mathbf{Q} \in \text{Ball}(\mathbf{P}, s(\epsilon)) \cap \mathcal{M}_r$. For any given $\mathbf{Z} \in \text{Ball}(\mathbf{P}, s(\epsilon))$, there are two cases: $\mathbf{Z} \in \mathcal{M}_r$ and $\mathbf{Z} \notin \mathcal{M}_r$. When $\mathbf{Z} \in \mathcal{M}_r$, by using Lemma 3.3 (i) with $\mathcal{C} = \mathbf{Q}$ and $\mathbf{D} = \mathbf{Z} = \pi_1(\mathbf{Z})$, (14) follows.

Next we consider $\mathbf{Z} \notin \mathcal{M}_r$. In this case, we set $\mathbf{C} = \mathbf{Q}$ and $\mathbf{D} = P_{T_{\mathcal{M}_r}(\mathbf{Q})}(\mathbf{Z})$. As $\mathbf{Z} \in \text{Ball}(\mathbf{P}, s(\epsilon))$ and $P_{T_{\mathcal{M}_r}(\mathbf{Q})}(\mathbf{Z}) \in \text{Ball}(\mathbf{P}, s_1(\epsilon))$. By using Lemma 3.3 (ii), we have

$$\|P_{T_{\mathcal{M}_r}(\mathbf{Q})}(\mathbf{Z}) - \pi_1(P_{T_{\mathcal{M}_r}(\mathbf{Q})}(\mathbf{Z}))\|_F \leq \epsilon \|P_{T_{\mathcal{M}_r}(\mathbf{Q})}(\mathbf{Z}) - \mathbf{Q}\|_F.$$

It implies that the set

$$\mathcal{M}_r \cap \text{Ball}(P_{T_{\mathcal{M}_r}(\mathbf{Q})}(\mathbf{Z}), \epsilon \|P_{T_{\mathcal{M}_r}(\mathbf{Q})}(\mathbf{Z}) - \mathbf{Q}\|_F)$$

is not void and is included in $Ball(\mathbf{Z}, \|\mathbf{Z} - \mathbf{Z}_1\|_F + \epsilon\|\mathbf{Z}_1 - \mathbf{Q}\|_F)$ with $\mathbf{Z}_1 = P_{T_{\mathcal{M}_r}(\mathbf{Q})}(\mathbf{Z})$. Note that $\pi_1(\mathbf{Z})$ is on the manifold \mathcal{M}_r and is included in $Ball(\mathbf{P}, s_1(\epsilon))$. By using Lemma 3.3 (i) (set $\mathbf{C} = \mathbf{Q}$ and $\mathbf{D} = \pi_1(\mathbf{Z})$), we have

$$\|\pi_1(\mathbf{Z}) - P_{T_{\mathcal{M}_r}(\mathbf{Q})}(\pi_1(\mathbf{Z}))\|_F \leq \epsilon\|\pi_1(\mathbf{Z}) - \mathbf{Q}\|_F. \quad (26)$$

Here the three points $\pi_1(\mathbf{Z})$, $P_{T_{\mathcal{M}_r}(\mathbf{Q})}(\pi_1(\mathbf{Z}))$ and \mathbf{Q} form a right triangle, we have

$$\begin{aligned} & \|\pi_1(\mathbf{Z}) - P_{T_{\mathcal{M}_r}(\mathbf{Q})}(\pi_1(\mathbf{Z}))\|_F^2 + \|P_{T_{\mathcal{M}_r}(\mathbf{Q})}(\pi_1(\mathbf{Z})) - \mathbf{Q}\|_F^2 \\ &= \|\pi_1(\mathbf{Z}) - \mathbf{Q}\|_F^2. \end{aligned}$$

By using this equality in the calculation of (26), we obtain

$$\begin{aligned} & \|\pi_1(\mathbf{Z}) - P_{T_{\mathcal{M}_r}(\mathbf{Q})}(\pi_1(\mathbf{Z}))\|_F \\ &= \sqrt{\|\pi_1(\mathbf{Z}) - \mathbf{Q}\|_F^2 - \|P_{T_{\mathcal{M}_r}(\mathbf{Q})}(\pi_1(\mathbf{Z})) - \mathbf{Q}\|_F^2} \\ &\leq \varphi(\epsilon)\|P_{T_{\mathcal{M}_r}(\mathbf{Q})}(\pi_1(\mathbf{Z})) - \mathbf{Q}\|_F, \end{aligned} \quad (27)$$

with $\varphi(\epsilon) = \frac{\epsilon}{\sqrt{1-\epsilon^2}}$. As $\mathbf{Z}_1 = P_{T_{\mathcal{M}_r}(\mathbf{Q})}(\mathbf{Z})$, we know that $(\mathbf{Z} - \mathbf{Z}_1) \perp T_{\mathcal{M}_r}(\mathbf{Q})$. By using $P_{T_{\mathcal{M}_r}(\mathbf{Q})}(\pi_1(\mathbf{Z})) \in T_{\mathcal{M}_r}(\mathbf{Q})$, we find that $P_{T_{\mathcal{M}_r}(\mathbf{Q})}(\pi_1(\mathbf{Z}))$, \mathbf{Z}_1 and \mathbf{Z} form a right-angled triangle which is included in $Ball(\mathbf{Z}, \|\mathbf{Z} - \mathbf{Z}_1\|_F + \epsilon\|\mathbf{Z}_1 - \mathbf{Q}\|_F)$. It implies that

$$\begin{aligned} & \|P_{T_{\mathcal{M}_r}(\mathbf{Q})}(\pi_1(\mathbf{Z})) - \mathbf{Z}_1\|_F \\ &\leq \|\mathbf{Z} - P_{T_{\mathcal{M}_r}(\mathbf{Q})}(\pi_1(\mathbf{Z}))\|_F \leq \|\mathbf{Z} - \mathbf{Z}_1\|_F + \epsilon\|\mathbf{Z}_1 - \mathbf{Q}\|_F, \end{aligned}$$

and

$$\begin{aligned} & \|P_{T_{\mathcal{M}_r}(\mathbf{Q})}(\pi_1(\mathbf{Z})) - \mathbf{Q}\|_F \\ &= \|P_{T_{\mathcal{M}_r}(\mathbf{Q})}(\pi_1(\mathbf{Z})) - \mathbf{Z}_1 + \mathbf{Z}_1 - \mathbf{Q}\|_F \\ &\leq \|P_{T_{\mathcal{M}_r}(\mathbf{Q})}(\pi_1(\mathbf{Z})) - \mathbf{Z}_1\|_F + \|\mathbf{Z}_1 - \mathbf{Q}\|_F \\ &< \|\mathbf{Z} - \mathbf{Z}_1\|_F + \epsilon\|\mathbf{Z}_1 - \mathbf{Q}\|_F + \|\mathbf{Z}_1 - \mathbf{Q}\|_F. \end{aligned} \quad (28)$$

By combing (27) and (28) with $0 < \epsilon < \frac{3}{5}$, we derive

$$\begin{aligned} & \|\pi_1(\mathbf{Z}) - P_{T_{\mathcal{M}_r}(\mathbf{Q})}(\pi_1(\mathbf{Z}))\|_F \\ &< \varphi(\epsilon)((1 + \epsilon)\|\mathbf{Z}_1 - \mathbf{Q}\|_F + \|\mathbf{Z} - \mathbf{Z}_1\|_F) \\ &< 2\epsilon(\|\mathbf{Z}_1 - \mathbf{Q}\|_F + \|\mathbf{Z} - \mathbf{Z}_1\|_F). \end{aligned}$$

Now we set \mathbf{Z}_2 as the reflection point of $\pi_1(\mathbf{Z})$ with respect to the tangent space $T_{\mathcal{M}_r}(\mathbf{Q})$. It is clear that

$$\|\pi_1(\mathbf{Z}) - P_{T_{\mathcal{M}_r}(\mathbf{Q})}(\pi_1(\mathbf{Z}))\|_F = \|P_{T_{\mathcal{M}_r}(\mathbf{Q})}(\pi_1(\mathbf{Z})) - \mathbf{Z}_2\|_F.$$

Along the direction of $\mathbf{Z} - \mathbf{Z}_1$, we can find a point \mathbf{Z}_3 such that

$$\|\mathbf{Z}_1 - \mathbf{Z}_3\|_F = \|\pi_1(\mathbf{Z}) - P_{T_{\mathcal{M}_r}(\mathbf{Q})}(\pi_1(\mathbf{Z}))\|_F.$$

Thus we can estimate the distance between $P_{T_{\mathcal{M}_r}(\mathbf{Q})}(\mathbf{Z})$ and $P_{T_{\mathcal{M}_r}(\mathbf{Q})}(\pi_1(\mathbf{Z}))$ as follows:

$$\begin{aligned} & \|P_{T_{\mathcal{M}_r}(\mathbf{Q})}(\mathbf{Z}) - P_{T_{\mathcal{M}_r}(\mathbf{Q})}(\pi_1(\mathbf{Z}))\|_F^2 \\ &= \|\mathbf{Z} - \mathbf{Z}_2\|_F^2 - \|\mathbf{Z} - \mathbf{Z}_3\|_F^2 \\ &\leq (\|\mathbf{Z} - \mathbf{Z}_1\|_F + \epsilon\|\mathbf{Z}_1 - \mathbf{Q}\|_F)^2 \\ &\quad - (\|\mathbf{Z} - \mathbf{Z}_1\|_F - 2\epsilon(\|\mathbf{Z}_1 - \mathbf{Q}\|_F + \|\mathbf{Z} - \mathbf{Z}_1\|_F))^2 \\ &= (\|\mathbf{Z} - \mathbf{Z}_1\|_F + \epsilon\|\mathbf{Z}_1 - \mathbf{Q}\|_F)^2 \\ &\quad - ((1 - 2\epsilon)\|\mathbf{Z} - \mathbf{Z}_1\|_F - 2\epsilon\|\mathbf{Z}_1 - \mathbf{Q}\|_F)^2. \end{aligned}$$

With the above inequalities, for any given $\mathbf{Z} \in Ball(\mathbf{P}, s(\epsilon))$, we have

$$\begin{aligned} & \|\pi_1(\mathbf{Z}) - P_{T_{\mathcal{M}_r}(\mathbf{Q})}(\mathbf{Z})\|_F^2 \\ &= \|P_{T_{\mathcal{M}_r}(\mathbf{Q})}(\mathbf{Z}) - P_{T_{\mathcal{M}_r}(\mathbf{Q})}(\pi_1(\mathbf{Z}))\|_F^2 \\ &\quad + \|\pi_1(\mathbf{Z}) - P_{T_{\mathcal{M}_r}(\mathbf{Q})}(\pi_1(\mathbf{Z}))\|_F^2 \\ &\leq (\|\mathbf{Z} - \mathbf{Z}_1\|_F + \epsilon\|\mathbf{Z}_1 - \mathbf{Q}\|_F)^2 - ((1 - 2\epsilon)\|\mathbf{Z} - \mathbf{Z}_1\|_F \\ &\quad - 2\epsilon\|\mathbf{Z}_1 - \mathbf{Q}\|_F)^2 + 4\epsilon^2(\|\mathbf{Z}_1\|_F + \|\mathbf{Z}_2\|_F)^2 \\ &= 2\epsilon\|\mathbf{Z} - \mathbf{Z}_1\|_F\|\mathbf{Z}_1 - \mathbf{Q}\|_F + \epsilon^2\|\mathbf{Z}_1 - \mathbf{Q}\|_F^2 \\ &\quad + 4\epsilon(\|\mathbf{Z} - \mathbf{Z}_1\|_F^2 + \|\mathbf{Z}_1 - \mathbf{Q}\|_F\|\mathbf{Z} - \mathbf{Z}_1\|_F) \\ &< 16\epsilon\|\mathbf{Z} - \mathbf{Q}\|_F. \end{aligned}$$

The second inequality is derived by using the facts that $\|\mathbf{Z}_1 - \mathbf{Q}\|_F < \|\mathbf{Z} - \mathbf{Q}\|_F$, $\|\mathbf{Z}_2 - \mathbf{Q}\|_F < \|\mathbf{Z} - \mathbf{Q}\|_F$ and $\epsilon^2 < \epsilon$. Hence the result follows. \square

A.2 Proof of Lemma 3.6

Proof. Note that $\pi_1(P_{T_{\mathcal{M}_r}(\mathbf{Q})}(\mathbf{Z}))$ and $\pi_1(\mathbf{Z})$ are on the manifold \mathcal{M}_r , and $\pi_1(P_{T_{\mathcal{M}_r}(\mathbf{Q})}(\mathbf{Z}))$ is the closest point to $P_{T_{\mathcal{M}_r}(\mathbf{Q})}(\mathbf{Z})$ on the manifold \mathcal{M}_r . Therefore, we have

$$\begin{aligned} & \|P_{T_{\mathcal{M}_r}(\mathbf{Q})}(\mathbf{Z}) - \pi_1(P_{T_{\mathcal{M}_r}(\mathbf{Q})}(\mathbf{Z}))\|_F \leq \\ & \|P_{T_{\mathcal{M}_r}(\mathbf{Q})}(\mathbf{Z}) - \pi_1(\mathbf{Z})\|_F. \end{aligned} \quad (29)$$

We remark that \mathcal{M}_{rn} is a smooth manifold [34] and $\mathbf{P} \in \mathcal{M}_{rn}$. Thus there exists an s' such that π is continuous on $Ball(\mathbf{P}, s')$. In other words, we can find a constant $\alpha > 0$ such that

$$\|\pi(\mathbf{X}) - \pi(\mathbf{X}')\|_F \leq \alpha\|\mathbf{X} - \mathbf{X}'\|_F, \forall \mathbf{X}, \mathbf{X}' \in Ball(\mathbf{P}, s'). \quad (30)$$

Now we choose $s_1(\epsilon)$ to be the minimum of s' and $s(\epsilon)$ in Lemmas 3.2 and 3.4. For all $\mathbf{Z} \in Ball(\mathbf{P}, s_1(\epsilon))$, we have

$$\begin{aligned} & \|\pi(\pi_1(P_{T_{\mathcal{M}_r}(\mathbf{Q})}(\mathbf{Z}))) - \pi(\mathbf{Z})\|_F \\ &= \|\pi(\pi_1(P_{T_{\mathcal{M}_r}(\mathbf{Q})}(\mathbf{Z}))) - \pi(\pi_1(\mathbf{Z})) + \pi(\pi_1(\mathbf{Z})) - \pi(\mathbf{Z})\|_F \\ &\leq \|\pi(\pi_1(P_{T_{\mathcal{M}_r}(\mathbf{Q})}(\mathbf{Z}))) - \pi(\pi_1(\mathbf{Z}))\|_F + \|\pi(\pi_1(\mathbf{Z})) - \pi(\mathbf{Z})\|_F \\ &\leq \alpha\|\pi_1(P_{T_{\mathcal{M}_r}(\mathbf{Q})}(\mathbf{Z})) - \pi_1(\mathbf{Z})\|_F + \epsilon_1(\epsilon)\|\mathbf{Z} - \pi(\mathbf{Z})\|_F \\ &\leq \alpha\|\pi_1(P_{T_{\mathcal{M}_r}(\mathbf{Q})}(\mathbf{Z})) - P_{T_{\mathcal{M}_r}(\mathbf{Q})}(\mathbf{Z})\|_F + \epsilon(\epsilon)\|\mathbf{Z} - \pi(\mathbf{Z})\|_F \\ &\quad + \alpha\|P_{T_{\mathcal{M}_r}(\mathbf{Q})}(\mathbf{Z}) - \pi_1(\mathbf{Z})\|_F \\ &\leq 2\alpha\|P_{T_{\mathcal{M}_r}(\mathbf{Q})}(\mathbf{Z}) - \pi_1(\mathbf{Z})\|_F + \epsilon(\epsilon)\|\mathbf{Z} - \pi(\mathbf{Z})\|_F \\ &\leq 8\alpha\sqrt{\epsilon}\|\mathbf{Z} - \mathbf{Q}\|_F + \epsilon(\epsilon)\|\mathbf{Z} - \pi(\mathbf{Z})\|_F \\ &\leq (\epsilon(\epsilon) + 8\alpha\sqrt{\epsilon})\|\mathbf{Z} - \pi(\mathbf{Z})\|_F + 8\alpha\sqrt{\epsilon}\|\mathbf{Q} - \pi(\mathbf{Z})\|_F. \end{aligned}$$

The second inequality is derived by (30) and (13), the fourth inequality is derived by (29) and the fifth inequality is derived by (14). We choose $\epsilon_1(\epsilon) = \epsilon(\epsilon) + 8\alpha\sqrt{\epsilon}$ and $\epsilon_2(\epsilon) = 8\alpha\sqrt{\epsilon}$. The result follows. \square

A.3 Proof of Lemma 3.7

Proof. Without loss of generality, we can assume $\pi(\mathbf{Z}) = 0$, thus it is sufficient to prove

$$\|\pi_1(P_{T_{\mathcal{M}_r}(\mathbf{Q})}(\mathbf{Z}))\|_F < c\|\mathbf{Z}\|_F \quad \text{or} \quad \frac{\pi_1(P_{T_{\mathcal{M}_r}(\mathbf{Q})}(\mathbf{Z}))\|_F}{\|\mathbf{Z}\|_F} < c$$

is satisfied. By the definition of $\sigma(\mathbf{P})$, we can find a constant c_1 such that $\sigma(\mathbf{P}) < c_1 < c$. Note that $\sigma(\cdot)$ is

a local continuous function, it implies that there exist a constant s_1 such that $\sigma(\mathbf{S}) < c_1$ is satisfied for every point $\mathbf{S} \in \mathcal{M}_{r_n} \cap \text{Ball}(\mathbf{P}, s_1)$. Let $s < s_1$. Since $\pi(\cdot)$ is a local continuous function, $\pi(\mathbf{Z}) \in \mathcal{M}_{r_n} \cap \text{Ball}(\mathbf{P}, s)$, thus we have $\sigma(\pi(\mathbf{Z})) = \sigma(0) < c_1$. Now we set $\mathbf{D} = \pi_1(\mathbf{Z})$, $\mathbf{D}' = P_{T_{\mathcal{M}_r}(\pi(\mathbf{Z}))}(\mathbf{Z})$ and $\mathbf{E} = \pi_1(P_{T_{\mathcal{M}_r}(\mathbf{Q})}(\mathbf{Z}))$, then we have

$$\frac{\|\pi_1(P_{T_{\mathcal{M}_r}(\mathbf{Q})}(\mathbf{Z}))\|_F}{\|\mathbf{Z}\|_F} = \frac{\|\mathbf{E}\|_F}{\|\mathbf{Z}\|_F} = \left(\frac{\|\mathbf{E}\|_F}{\|\mathbf{D}'\|_F} \right) \left(\frac{\|\mathbf{D}'\|_F}{\|\mathbf{Z}\|_F} \right).$$

The remaining task is to estimate the values of $\frac{\|\mathbf{E}\|_F}{\|\mathbf{D}'\|_F}$ and $\frac{\|\mathbf{D}'\|_F}{\|\mathbf{Z}\|_F}$. Recall that \mathcal{M}_n is a linear affine manifold, and \mathbf{Z} is on \mathcal{M}_n , it implies that $\mathbf{Z} = \pi_2(\mathbf{Z}) = P_{T_{\mathcal{M}_n}(\pi(\mathbf{Z}))}(\mathbf{Z})$. Therefore,

$$\begin{aligned} \|\mathbf{D}'\|_F &= \|P_{T_{\mathcal{M}_r}(\pi(\mathbf{Z}))}(\mathbf{Z})\|_F = \|P_{T_{\mathcal{M}_r}(\pi(\mathbf{Z}))}(\mathbf{Z}) - \pi(\mathbf{Z})\|_F \\ &= \sigma(\pi(\mathbf{Z})) \|P_{T_{\mathcal{M}_n}(\pi(\mathbf{Z}))}(\mathbf{Z})\|_F, \end{aligned}$$

and thus $\frac{\|\mathbf{D}'\|_F}{\|\mathbf{Z}\|_F} = \sigma(\pi(\mathbf{Z})) = \sigma(0) < c_1$.

In order to estimate $\frac{\|\mathbf{E}\|_F}{\|\mathbf{D}'\|_F}$, we consider $\|\mathbf{E} - \mathbf{D}'\|_F$ which can be bounded by the following inequality:

$$\begin{aligned} &\|\mathbf{E} - \mathbf{D}'\|_F \\ &= \|\mathbf{E} - \mathbf{D} + \mathbf{D} - \mathbf{D}'\|_F \leq \|\mathbf{E} - \mathbf{D}\|_F + \|\mathbf{D} - \mathbf{D}'\|_F \\ &= \|\mathbf{E} - P_{T_{\mathcal{M}_r}(\mathbf{Q})}(\mathbf{Z}) + P_{T_{\mathcal{M}_r}(\mathbf{Q})}(\mathbf{Z}) - \mathbf{D}\|_F + \|\mathbf{D} - \mathbf{D}'\|_F \\ &\leq \|\mathbf{E} - P_{T_{\mathcal{M}_r}(\mathbf{Q})}(\mathbf{Z})\|_F + \|P_{T_{\mathcal{M}_r}(\mathbf{Q})}(\mathbf{Z}) - \mathbf{D}\|_F \\ &\quad + \|\mathbf{D} - \mathbf{D}'\|_F \\ &= \|\pi_1(P_{T_{\mathcal{M}_r}(\mathbf{Q})}(\mathbf{Z})) - P_{T_{\mathcal{M}_r}(\mathbf{Q})}(\mathbf{Z})\|_F \\ &\quad + \|P_{T_{\mathcal{M}_r}(\mathbf{Q})}(\mathbf{Z}) - \pi_1(\mathbf{Z})\|_F + \|\mathbf{D} - \mathbf{D}'\|_F. \end{aligned} \quad (31)$$

By using Lemma 3.4 and $\mathbf{Z} = \pi_2(\mathbf{Q})$ is the closest point to \mathbf{Q} with respect to $\pi_2(\cdot)$,

$$\begin{aligned} \|P_{T_{\mathcal{M}_r}(\mathbf{Q})}(\mathbf{Z}) - \pi_1(\mathbf{Z})\|_F &< 4\sqrt{\epsilon} \|\mathbf{Z} - \mathbf{Q}\|_F \\ &\leq 4\sqrt{\epsilon} \|\mathbf{Q} - \pi(\mathbf{Z})\|_F. \end{aligned} \quad (32)$$

By using the fact that $\pi_1(P_{T_{\mathcal{M}_r}(\mathbf{Q})}(\mathbf{Z}))$ is the closest point to $P_{T_{\mathcal{M}_r}(\mathbf{Q})}(\mathbf{Z})$ with respect to $\pi_1(\cdot)$ and (32), we have

$$\begin{aligned} &\|\pi_1(P_{T_{\mathcal{M}_r}(\mathbf{Q})}(\mathbf{Z})) - P_{T_{\mathcal{M}_r}(\mathbf{Q})}(\mathbf{Z})\|_F \\ &\leq \|P_{T_{\mathcal{M}_r}(\mathbf{Q})}(\mathbf{Z}) - \pi_1(\mathbf{Z})\|_F \leq 4\sqrt{\epsilon} \|\mathbf{Q} - \pi(\mathbf{Z})\|_F. \end{aligned} \quad (33)$$

By applying Lemma 3.2 on $\|\mathbf{D} - \mathbf{D}'\|_F$, we get

$$\|\mathbf{D} - \mathbf{D}'\|_F = \|P_{T_{\mathcal{M}_r}(\pi(\mathbf{Z}))}(\mathbf{Z}) - \pi_1(\mathbf{Z})\|_F \leq 4\sqrt{\epsilon} \|\mathbf{Z}\|_F. \quad (34)$$

By putting (32), (33) and (34) into (31), we obtain the following estimate

$$\begin{aligned} &\|\mathbf{E} - \mathbf{D}'\|_F \\ &< 4\sqrt{\epsilon} \|\mathbf{Q} - \pi(\mathbf{Z})\|_F + 4\sqrt{\epsilon} \|\mathbf{Q} - \pi(\mathbf{Z})\|_F \\ &\quad + 4\sqrt{\epsilon} \|\mathbf{Z} - \pi(\mathbf{Z})\|_F \\ &= 8\sqrt{\epsilon} \|\mathbf{Q} - \pi(\mathbf{Z})\|_F + 4\sqrt{\epsilon} \|\mathbf{Z} - \mathbf{Q} + \mathbf{Q} - \pi(\mathbf{Z})\|_F \\ &\leq 8\sqrt{\epsilon} \|\mathbf{Q} - \pi(\mathbf{Z})\|_F + 4\sqrt{\epsilon} (\|\mathbf{Z} - \mathbf{Q}\|_F + \|\mathbf{Q} - \pi(\mathbf{Z})\|_F) \\ &< 8\sqrt{\epsilon} \|\mathbf{Q} - \pi(\mathbf{Z})\|_F + 8\sqrt{\epsilon} \|\mathbf{Q} - \pi(\mathbf{Z})\|_F \\ &= 16\sqrt{\epsilon} \|\mathbf{Q} - \pi(\mathbf{Z})\|_F. \end{aligned} \quad (35)$$

Now we choose $c_2 > 1$ such that $c_2 c_1 < c$, and also sufficiently small $\epsilon \in (0, \frac{3}{5})$ such that

$$16\sqrt{\epsilon} \left(\frac{c_2}{c_2 - 1} \right) \|\mathbf{Q}\|_F < c \|\mathbf{Z}\|_F \quad (36)$$

is satisfied. For the value of $\frac{\|\mathbf{E}\|_F}{\|\mathbf{D}'\|_F}$, there are two cases to be considered: $\frac{\|\mathbf{E}\|_F}{\|\mathbf{D}'\|_F} \leq c_2$ or $\frac{\|\mathbf{E}\|_F}{\|\mathbf{D}'\|_F} > c_2$. For the first case, it is easy to check

$$\frac{\|\mathbf{E}\|_F}{\|\mathbf{Z}\|_F} = \frac{\|\mathbf{E}\|_F}{\|\mathbf{D}'\|_F} \frac{\|\mathbf{D}'\|_F}{\|\mathbf{Z}\|_F} < c_2 c_1 < c.$$

For the second case, $\frac{\|\mathbf{E}\|_F}{\|\mathbf{D}'\|_F} > c_2$. By using (35), we derive

$$\|\mathbf{E}\|_F - \|\mathbf{D}'\|_F \leq \|\mathbf{E} - \mathbf{D}'\|_F < 16\sqrt{\epsilon} \|\mathbf{Q}\|_F.$$

or $\|\mathbf{D}'\|_F > \|\mathbf{E}\|_F - 16\sqrt{\epsilon} \|\mathbf{Q}\|_F$. It implies that

$$c_2 < \frac{\|\mathbf{E}\|_F}{\|\mathbf{D}'\|_F} < \frac{\|\mathbf{E}\|_F}{\|\mathbf{E}\|_F - 16\sqrt{\epsilon} \|\mathbf{Q}\|_F}.$$

By using (36), we have

$$\frac{\|\mathbf{E}\|_F}{\|\mathbf{Z}\|_F} < \frac{\left(\frac{c_2}{c_2 - 1} \right) 16\sqrt{\epsilon} \|\mathbf{Q}\|_F}{\|\mathbf{Z}\|_F} < c.$$

The results follow. \square

REFERENCES

- [1] K. Chen, *Matrix preconditioning techniques and applications*. Cambridge University Press, 2005, vol. 19.
- [2] M. Chen, W.-S. Chen, B. Chen, and B. Pan, "Non-negative sparse representation based on block nmf for face recognition," in *Chinese Conference on Biometric Recognition*. Springer, 2013, pp. 26–33.
- [3] C. Ding, X. He, and H. D. Simon, "On the equivalence of nonnegative matrix factorization and spectral clustering," in *Proceedings of the 2005 SIAM International Conference on Data Mining*. SIAM, 2005, pp. 606–610.
- [4] C. Ding, T. Li, W. Peng, and H. Park, "Orthogonal nonnegative matrix t-factorizations for clustering," in *Proceedings of the 12th ACM SIGKDD International Conference on Knowledge Discovery and Data Mining*, 2006, pp. 126–135.
- [5] D. Guillamet and J. Vitria, "Non-negative matrix factorization for face recognition," in *Catalonian Conference on Artificial Intelligence*. Springer, 2002, pp. 336–344.
- [6] D. Guillamet, J. Vitria, and B. Schiele, "Introducing a weighted non-negative matrix factorization for image classification," *Pattern Recognition Letters*, vol. 24, no. 14, pp. 2447–2454, 2003.
- [7] L. Jing, J. Yu, T. Zeng, and Y. Zhu, "Semi-supervised clustering via constrained symmetric non-negative matrix factorization," in *International Conference on Brain Informatics*. Springer, 2012, pp. 309–319.
- [8] D. D. Lee and H. S. Seung, "Learning the parts of objects by non-negative matrix factorization," *Nature*, vol. 401, no. 6755, pp. 788–791, 1999.
- [9] J. Liu, Z. Wu, Z. Wei, L. Xiao, and L. Sun, "A novel sparsity constrained nonnegative matrix factorization for hyperspectral unmixing," in *2012 IEEE International Geoscience and Remote Sensing Symposium*. IEEE, 2012, pp. 1389–1392.
- [10] Y. Liu, X.-Z. Pan, R.-J. Shi, Y.-L. Li, C.-K. Wang, and Z.-T. Li, "Predicting soil salt content over partially vegetated surfaces using non-negative matrix factorization," *IEEE Journal of Selected Topics in Applied Earth Observations and Remote Sensing*, vol. 8, no. 11, pp. 5305–5316, 2015.
- [11] Y. Wang, Y. Jia, C. Hu, and M. Turk, "Non-negative matrix factorization framework for face recognition," *International Journal of Pattern Recognition and Artificial Intelligence*, vol. 19, no. 04, pp. 495–511, 2005.
- [12] D. Zhang, S. Chen, and Z.-H. Zhou, "Two-dimensional non-negative matrix factorization for face representation and recognition," in *International Workshop on Analysis and Modeling of Faces and Gestures*. Springer, 2005, pp. 350–363.
- [13] M. W. Berry and J. Kogan, *Text mining: applications and theory*. John Wiley & Sons, 2010.
- [14] T. Li and C. Ding, "The relationships among various nonnegative matrix factorization methods for clustering," in *Sixth International Conference on Data Mining (ICDM'06)*. IEEE, 2006, pp. 362–371.

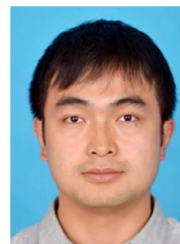
- [15] V. P. Pauca, F. Shahnaz, M. W. Berry, and R. J. Plemmons, "Text mining using non-negative matrix factorizations," in *Proceedings of the 2004 SIAM International Conference on Data Mining*. SIAM, 2004, pp. 452–456.
- [16] W. Xu, X. Liu, and Y. Gong, "Document clustering based on non-negative matrix factorization," in *Proceedings of the 26th Annual International ACM SIGIR Conference on Research and Development in Informaion Retrieval*, 2003, pp. 267–273.
- [17] A. Cichocki, R. Zdunek, A. H. Phan, and S.-i. Amari, *Nonnegative matrix and tensor factorizations: applications to exploratory multi-way data analysis and blind source separation*. John Wiley & Sons, 2009.
- [18] P. M. Kim and B. Tidor, "Subsystem identification through dimensionality reduction of large-scale gene expression data," *Genome Research*, vol. 13, no. 7, pp. 1706–1718, 2003.
- [19] H. Kim and H. Park, "Sparse non-negative matrix factorizations via alternating non-negativity-constrained least squares for microarray data analysis," *Bioinformatics*, vol. 23, no. 12, pp. 1495–1502, 2007.
- [20] A. Pascual-Montano, J. M. Carazo, K. Kochi, D. Lehmann, and R. D. Pascual-Marqui, "Nonsmooth nonnegative matrix factorization (nsNMF)," *IEEE Transactions on Pattern Analysis and Machine Intelligence*, vol. 28, no. 3, pp. 403–415, 2006.
- [21] G. Wang, A. V. Kossenkov, and M. F. Ochs, "LS-NMF: a modified non-negative matrix factorization algorithm utilizing uncertainty estimates," *BMC Bioinformatics*, vol. 7, no. 1, p. 175, 2006.
- [22] P. Paatero and U. Tapper, "Positive matrix factorization: A non-negative factor model with optimal utilization of error estimates of data values," *Environmetrics*, vol. 5, no. 2, pp. 111–126, 1994.
- [23] A. Cichocki, R. Zdunek, and S.-i. Amari, "Hierarchical ALS algorithms for nonnegative matrix and 3D tensor factorization," in *International Conference on Independent Component Analysis and Signal Separation*. Springer, 2007, pp. 169–176.
- [24] S. Choi, "Algorithms for orthogonal nonnegative matrix factorization," in *2008 IEEE International Joint Verference on Neural Networks (IEEE World Congress on Computational Intelligence)*. IEEE, 2008, pp. 1828–1832.
- [25] N. Gillis and F. Glineur, "Accelerated multiplicative updates and hierarchical ALS algorithms for nonnegative matrix factorization," *Neural Computation*, vol. 24, no. 4, pp. 1085–1105, 2012.
- [26] N. Gillis and S. A. Vavasis, "Fast and robust recursive algorithms for separable nonnegative matrix factorization," *IEEE Transactions on Pattern Analysis and Machine Intelligence*, vol. 36, no. 4, pp. 698–714, 2013.
- [27] D. Kuang, C. Ding, and H. Park, "Symmetric nonnegative matrix factorization for graph clustering," in *Proceedings of the 2012 SIAM International Conference on Data Mining*. SIAM, 2012, pp. 106–117.
- [28] D. Kuang, S. Yun, and H. Park, "SymNMF: nonnegative low-rank approximation of a similarity matrix for graph clustering," *Journal of Global Optimization*, vol. 62, no. 3, pp. 545–574, 2015.
- [29] C.-J. Lin, "Projected gradient methods for nonnegative matrix factorization," *Neural Computation*, vol. 19, no. 10, pp. 2756–2779, 2007.
- [30] D. D. Lee and H. S. Seung, "Algorithms for non-negative matrix factorization," in *Advances in Neural Information Processing Systems*, 2001, pp. 556–562.
- [31] J. Pan and N. Gillis, "Generalized separable nonnegative matrix factorization," *IEEE Transactions on Pattern Analysis and Machine Intelligence*, 2019.
- [32] Z. Yuan and E. Oja, "Projective nonnegative matrix factorization for image compression and feature extraction," in *Scandinavian Conference on Image Analysis*. Springer, 2005, pp. 333–342.
- [33] G. R. Naik, *Non-negative matrix factorization techniques*. Springer, 2016.
- [34] G. Song and M. K. Ng, "Nonnegative low rank matrix approximation for nonnegative matrices," *Applied Mathematics Letters*, vol. 105, p. 106300, 2020.
- [35] B. Vandereycken, "Low-rank matrix completion by riemannian optimization," *SIAM Journal on Optimization*, vol. 23, no. 2, pp. 1214–1236, 2013.
- [36] G. H. Golub and C. F. Van Loan, *Matrix computations*. JHU press, 2012, vol. 3.
- [37] F. Andersson and M. Carlsson, "Alternating projections on non-tangential manifolds," *Constructive Approximation*, vol. 38, no. 3, pp. 489–525, 2013.
- [38] D. Cai, X. He, and J. Han, "Document clustering using locality preserving indexing," *IEEE Transactions on Knowledge and Data Engineering*, vol. 17, no. 12, pp. 1624–1637, 2005.
- [39] M. C. U. Araújo, T. C. B. Saldanha, R. K. H. Galvao, T. Yoneyama, H. C. Chame, and V. Visani, "The successive projections algorithm for variable selection in spectroscopic multicomponent analysis," *Chemometrics and Intelligent Laboratory Systems*, vol. 57, no. 2, pp. 65–73, 2001.
- [40] A. Vandaele, N. Gillis, Q. Lei, K. Zhong, and I. Dhillon, "Coordinate descent methods for symmetric nonnegative matrix factorization," *arXiv preprint arXiv:1509.01404*, 2015.
- [41] L. Zelnik-Manor and P. Perona, "Self-tuning spectral clustering," in *Advances in neural information processing systems*, 2005, pp. 1601–1608.
- [42] F. Zhu, Y. Wang, B. Fan, S. Xiang, G. Meng, and C. Pan, "Spectral unmixing via data-guided sparsity," *IEEE Transactions on Image Processing*, vol. 23, no. 12, pp. 5412–5427, 2014.
- [43] J. Pan, M. K. Ng, Y. Liu, X. Zhang, and H. Yan, "Orthogonal non-negative tucker decomposition," *arXiv preprint arXiv:1912.06836*, 2019.



Guang-Jing Song received the Ph.D. degree in mathematics from Shanghai University, Shanghai, China, in 2010. He is currently a professor of School of Mathematics and Information Sciences, Weifang University. His research interests include numerical linear algebra, sparse and low-rank modeling, tensor decomposition and multi-dimensional image processing.



Michael K. Ng is the Director of Research Division for Mathematical and Statistical Science, and Chair Professor of Department of Mathematics, the University of Hong Kong, and Chairman of HKU-TCL Joint Research Center for AI. His research areas are data science, scientific computing, and numerical linear algebra.



Tai-Xiang Jiang received the B.S., Ph.D. degrees in mathematics and applied mathematics from the University of Electronic Science and Technology of China (UESTC), Chengdu, China, in 2013. He is currently a lecturer with the School of Economic Information Engineering, Southwestern University of Finance and Economics. His research interests include sparse and low-rank modeling, tensor decomposition and multi-dimensional image processing. <https://sites.google.com/view/taixiangjiang/>